공학석사 학위논문

Pyrochemical Decontamination Process Development for the Volume Reduction of Intermediate Level Waste from PWR Decommissioning

가압경수로형 원자로 해체 후 발생된 중준위 폐기물의 부피감소를 위한 전해제염 공정 개발

2019년 2월

서울대학교 대학원

에너지시스템공학부

허정호

Abstract

Pyrochemical Decontamination Process Development for the Volume Reduction of Intermediate Level Waste from PWR Decommissioning

Jungho Hur

School of Energy Systems Engineering

The Graduate School

Seoul National University

Currently, 454 nuclear power plants are operating globally and account for about 11% of the total electric power generation. About 66% of these nuclear power plants have been in operation for more than 30 years, and the proportion of such old nuclear power plants is expected to continuously increase. In Korea, the Kori Unit #1 reactor has been decided to permanent shutdown, and 7 PWR reactors will reached the design life time before 2030. As a result, the need to prepare for the decommissioning of nuclear power plants is increasing, and the management of intermediate and low-level radioactive waste from decommissioning is also becoming important. Among them, the amount of the intermediate level metal waste from reactor internals periphery to reactor core is about 66 tons. The reactor internals are made of stainless steel and are exposed to high neutron flux for a long period. As the stainless steel is activated, long living activation products such as C^{14},

Nb^{94}, Ni^{59} and Ni^{63} and short living activation products such as Co^{60} are generated. However, according to the current regulations, intermediate level radioactive wastes containing a large amount of long living radionuclides can not be disposed of due to the total activity limits of Gyeongju repository. Therefore, most of the countries as well as Korea kept them in the interim storage on site and waiting for the construction of high-level radioactive waste or spent nuclear fuel repository. In order to solve this problem, it is necessary to develop decontamination technology for long living intermediate level wastes.

Based on ORIGEN-2 modeling with some assumptions, pressurized water reactor internals were modeled. The radioactivity of C^{14}, Nb^{94}, Ni^{59}, Ni^{63} and Co^{60} were 1.83E+06Bq/g, 2.88E+04Bq/g, 5.40E+06Bq/g, 1.05E+07Bq/g, 1.35E+09Bq/g, respectively. The decontamination factors required for disposal of all reactor internals from 20 units are 8.2, 259.1, 73.0, 94.7, and 36.6, respectively.

In this paper, electrorefining process that takes good advantage of theoretically very low secondary waste generation was suggested for decontamination process. LiCl-KCl eutectic salt, which has lower operating temperature than fluoride salt (LiF-KF) and has less corrosion problem, was used as electrolyte. Approach for electrorefining is recovering Fe and Cr with high tendency to oxidation by leaving long-living nuclides using standard potential difference between them.

In order to investigate the behavior of the major elements (Fe, Co, Ni, Cr) in the LiCl-KCl, cyclic voltammetry at 500°C was performed. All nuclides except for Cr showed a single pair of redox peak. Cr showed two pairs of redox peaks, but the oxidation peak of Fe was -0.2 ~ -0.1V

[vs. 1 wt. % Ag/AgCl]. The oxidation behavior between Cr^{2+} and Cr^{3+} was negligible in that region. Apparent reduction potentials and diffusion coefficients in molten salt were obtained based on the results of cyclic voltammetry. In addition, a database for related studies was constructed by acquiring exchange current density and charge transfer coefficient of each nuclide through Linear Polarization Method. The achievability of the decontamination factors through electrorefining was evaluated by conducting REFIN modeling, 1-D time dependent simulation code. It showed that decontamination factors for Nb and Co can be achieved through electrorefining. In case of Ni, it is possible to achieve decontamination factor by 2 successive electrorefining.

Electrorefining experiments were performed to verify the modeling results. LiCl-KCl-3 wt. % $FeCl_2$ was used as electrolyte, and a type 304 stainless steel rod was used as anode. During the experiment, baskets were installed around the anode to recover the metals that could come off from the anode and the cathode. The applied potential on anode were -0.2V[vs. 1 wt. % Ag/AgCl], -0.1V[vs. 1 wt. % Ag / AgCl], 0V[vs. 1 wt. % Ag/AgCl]. After electrorefining, the cathode surface, inside the baskets and bulk salts were analyzed by ICP-MS and XRD analysis was performed to confirm the deposition on cathode. As a result, it was confirmed that Fe was electrodeposited on the surface of the cathode and the decontamination factors of Co and Ni was decreased as the applied potential on anode was increased. However, in all three experiments, it was confirmed that the required decontamination factor can be satisfied when electrorefining process is repeated twice.

However, in the lab-scale electrorefining experiments, the problem of

the formation of the limiting current was confirmed and the new cell design was designed using the CFX code to overcome the issues. The design of new baskets in the cell was modeled as a porous structure, and the particle tracking and the IR drop modeling were performed. The IR drop between anode and cathode was more than 2 times greater than that of the non-porous baskets.

These findings suggest that if a pilot-scale electrorefiner is manufactured, it would result in reduction of 132.6 billion KRW economically.

Keywords: Reactor internals, Decommissioning waste, Stainless steel recycling, Molten Salt, Electrorefining

Student Number: 2017-24704

Contents

List of Tables

List of Figures

Chapter 1. Introduction

1.1 Background

Currently, 454 nuclear power plants are in operations to generate about 11% of world electricity and the two third of reactors have been operated over 30 years as shown in Figure 1.1 [1]. About 66% of nuclear power plants are pressurized water reactors (PWR) and already 50 of them were in permanent shutdown state.

In Korea, the Kori unit #1 which is the first PWR in Korea was permanently shut down in June 2017 and will be decommissioned under the management of Korea Hydro & Nuclear Power Company (KHNP). Furthermore, the 7 PWRs in Korea are also older than 30 years now and it indicates that the preparation of decommissioning plan for PWR including management plan for low-intermediate level waste (LILW) from decommissioning has to be established.

When decommissioning, intermediate level wastes (ILW) are generated from reactor vessel internal parts where the neutron flux level is high, especially the peripheral parts of reactor core. There are baffle, former, barrel and thermal shield that are significantly activated by high neutron flux. In Kori unit #1, the amount of activated metal wastes from reactor internals is about 300 tons and mass of ILW (baffle, former, barrel, thermal shield) is about 66 tons as shown in Table 1.1 [2]. ILW metal wastes from reactor internals will be stored in interim storage on

decommissioned site until new national repository for ILW or high level waste (HLW) can be established because long-living activation products are contained.

Most reactor internals are made of austenitic type 304 stainless steel which is a corrosion resistant steel alloy containing chromium, nickel and other elements. Austenitic stainless steels have a good combination of strength and corrosion resistance in extremely hot environments like nuclear reactor. The austenitic steels perform better than ferritic steels in the hot condition.

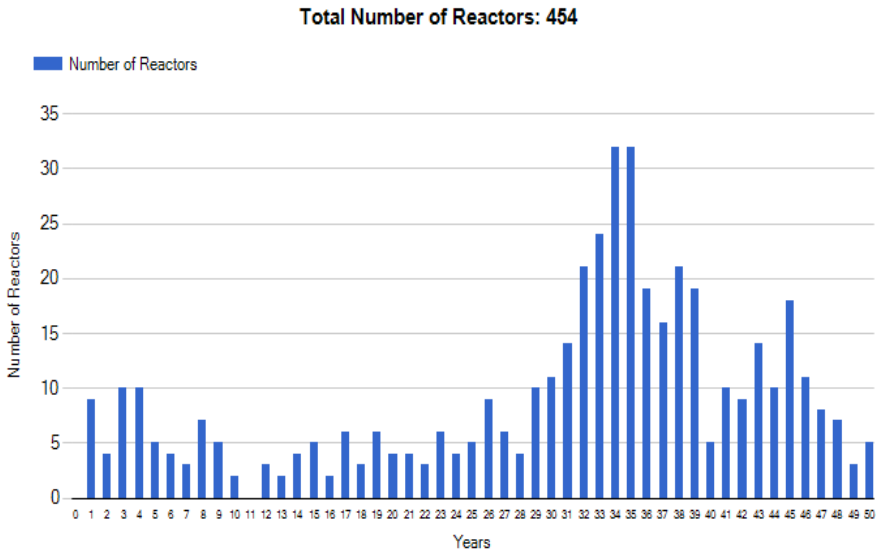

Figure 1.1 Age distribution of operating nuclear power plants worldwide as of 2019 [1].

Table 1.1 Estimated waste class of reactor vessel and internals from Kori unit #1 PWR nuclear power plant [2].

Components		Material	Waste class	Mass(Kg)
Side Parts of Rx Core	Baffle Plate	SS-304	ILW	9,523
	Barrel	SS-304	ILW	30,472
	Baffle Former	SS-304	ILW	2,612
	Thermal Shield	SS-304	ILW	23,697
Upper Parts of Rx Core	Upper Support Assembly	SS-304	VLLW	6,153
	Upper Core Plate	SS-304	LLW	1,534
	Guide Tube	SS-304	VLLW	8,419
	Upper Support Column	SS-304	VLLW	20,713
	Thermo-Couple Column	SS-304	VLLW	45
	Hold Down Spring	SS-304	VLLW	618
Lower Parts of Rx Core	Lower Core Plate	SS-304	LLW	1,682
	Core Support Plate	SS-304	VLLW	4,192
	Secondary Core Support Plate	SS-304	VLLW	1,284
	Secondary Core Support Column	SS-304	VLLW	7,776
	Core Support Tube	SS-304	VLLW	665
Reactor Pressure Vessel (RPV)		Low alloy Steel	LLW	185,397
Bio-shield (concrete)		Concrete	LLW	543,301
			VLLW	414,173

1.2 Problem Statement

The Korea's first of LILW disposal repository was constructed in Gyeongju and started operation in 2014 with disposal capacity of 100,000 drums. The Gyeongju repository will expand the capacity up to 800,000 drums step by step. Even after the expansion, ILW including reactor internals from decommissioning can not be directly disposed to the repository due to long-living activation products. When estimation on radioactivity of ILW from reactor internals after 15 years cooling was estimated by ORIGEN-2 code, the specific radioactivity of C^{14}, Nb^{94}, Ni^{59}, Ni^{63} and Co^{60} are respectively 1.83E+06Bq/g, 2.88E+04Bq/g, 5.4E+06Bq/g, 1.05E+09Bq/g and 1.35E+09Bq/g. It is obvious that the specific radioactivity of above nuclides are orders of magnitude higher than the radioactivity limit of Gyeongju repository. The more important fact is that amount of ILW which can be disposed to repository is limited by the total activity limit of facility. The first stage of LILW disposal facility has a limit for activity capacity of C^{14}, Nb^{94}, Ni^{59}, Ni^{63} and Co^{60} are respectively 1.66E+14Bq, 9.72E+10Bq, 3.78E+13Bq, 2.71E+15Bq and 1.03E+15Bq. From the ratio calculation as follow, amount of possibly disposed wastes can be calculated.

Amount of possibly disposed wastes from reactor internals=
Total activity limit [Bq] / Specific radioactivity of nuclide [Bq/g] (1.1)

From the calculation, it is shown that limits by C^{14}, Nb^{94}, Ni^{59}, Ni^{63} and Co^{60} are respectively 90.7tons, 3.38tons, 7tons, 2.58tons and 0.76tons. Co^{60} limit, however, is not important because of its short half-life. The limits by C^{14}, Nb^{94}, Ni^{59} and Ni^{63} show very important fact that ILW of reactor internals from decommissioning can not be directly disposed to Gyeongju repository, due to Nb and Ni as well as C.

It is remarkable to note that these three elements account for only 15% of total mass. It means that if 15% is separated from remaining, 85% can be classified as low level waste (LLW) that can be disposed of at Gyeongju repository.

Long-living intermediate level waste (LL-ILW) must be disposed of at ILW repository. Many counties including Korea store LL-ILW on site and without repository together like a Figure 1.2. If Korea follows the basic plan for Spent Nuclear fuel Management (MOTIE, 2016), it will be 2051 when a HLW repository is established. But if molten-salted based electrochemical separation process is applied to the above ILW, only 15% of ILW can be stored on site, alleviating the burden significantly, which can solve root as shown in Figure 1.3.

Table 1.2 Limited disposal quantity of ILW waste by total activity limit of Gyeongju repository.

Nuclide (Half-life)	Radioactivity (Bq/g)	Radioactivity limit (Bq/g)	Total activity limit (Bq)	Limited quantity for Gyeongju repository (tons)
H^{3} (12.3Y)	6.17E+05	1.11E+06	1.37E+15	2.22E+03
C^{14} (5730Y)	1.83E+06	2.22E+05	1.66E+14	9.07E+01
Nb^{94} (20000Y)	2.88E+04	1.11E+02	9.72E+10	3.37E+00
Ni^{59} (76000Y)	5.40E+06	7.40E+04	3.78E+13	7.00E+00
Ni^{63} (100Y)	1.05E+09	1.11E+07	2.71E+15	2.58E+00
Co^{60} (5.3Y)	1.35E+09	3.7E+07	1.03E+15	7.63E-01
Tc^{99} (213000Y)	1.03E+03	1.11E+03	7.85E+11	7.62E+02

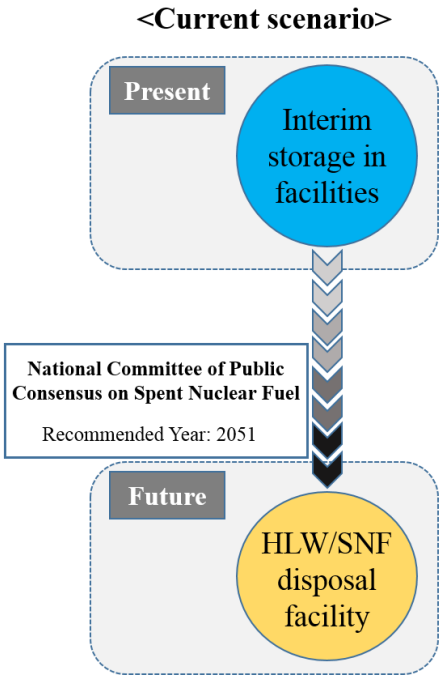

Figure 1.2 Current disposal scenario of LL-ILW in Korea.

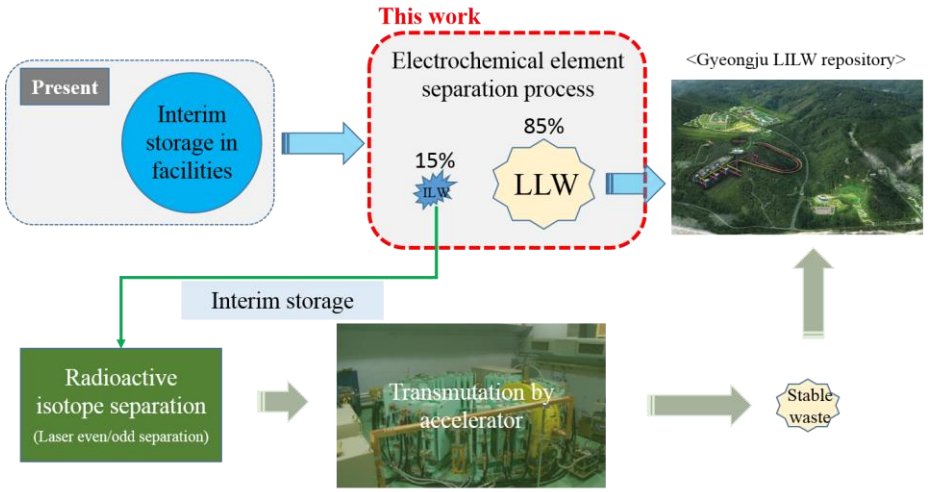

Figure 1.3 Potential roadmap of LL-ILW disposal with electrochemical separation process.

Current decontamination technologies are mainly focused on surface decontamination of metal wastes such as steam generator and pipes with activation products or surface. Surface decontamination process using foam or gel is very simple and being widely used. Mechanical decontamination process removes contaminated layers on surface tightly, taking advantage of shorter processing time.

Aqueous decontamination process using acid electrolyte is also being used but it needs large bath size on site. Methods described before are quite simple and effective for surface decontamination.However, they produce large secondary wastes.

There is also volumetric decontamination process using melting methodology being widely studied in many countries. But it is only effective for low level and big size metal wastes because this method is sort of homogenization process spreading radioactive elements from surface to whole volume. It will not be a fundamental solution for decontamination of ILW [3,4].

Table 1.3 Pros and cons of current decontamination methods.

		Pros	Cons
Surface decontamination [3]	Chemical decontamination	- Simple and a lot of experience	- Large secondary liquid waste - Effective is low for hidden surface
	Mechanical decontamination	- Remove tightly adherent material and fast	- Large secondary liquid waste - Base metal loss and dust contamination
	Electrochemical decontamination (Acid based, Wet)	- Secondary liquid waste is relatively low (chemical)	- Large bath size on site
Volumetric decontamination	Melting decontamination [4]	- Inaccessible surface is eliminated - Homogenization	- Only for low level and big size metal waste
	Electrochemical decontamination (Molten Salt based, dry)	- Ideally no secondary waste - No base metal loss and dust contamination	- Not deeply studied yet

Chapter 2. Literature Review

2.1 Electrochemistry of Decontamination

There are several electrochemical methods to study basic redox behavior of metallic elements in electrolyte. Among them, cyclic voltammetry (CV) is an electrochemical technique which measures the resulting current between the working electrode and counter electrode under the conditions where a working electrode potential is cycling. This technique is easy to figure out the reduction and oxidation peaks.

Experimental setup of CV is commonly consisted of three electrodes including working electrode, counter electrode and reference electrode. Working electrode potential is measured against reference electrode kept a constant potential under given condition. An applied potential on working electrode is linearly changed versus time. Redox reactions occur at the electrode surface with the change of potential. Reduction peak appears in the negative current region and oxidation peak is shown in the positive current region as shown in Figure 2.1 [5]. Data from CV is generally plotted as current versus applied potential.

In Figure 2.2 [5], increasing potential is applied during initial scan from t_0 to t_1 so that cathodic current occurs. After the reduction potential is reached at some point, cathodic current will decrease as the concentration of reducible ion is decreased. Then, the reverse scan from

t_1 to t_2 follows. During that time, reducible ion will be re-oxidized, giving increasing anodic current and anodic potential will be reached as follows.

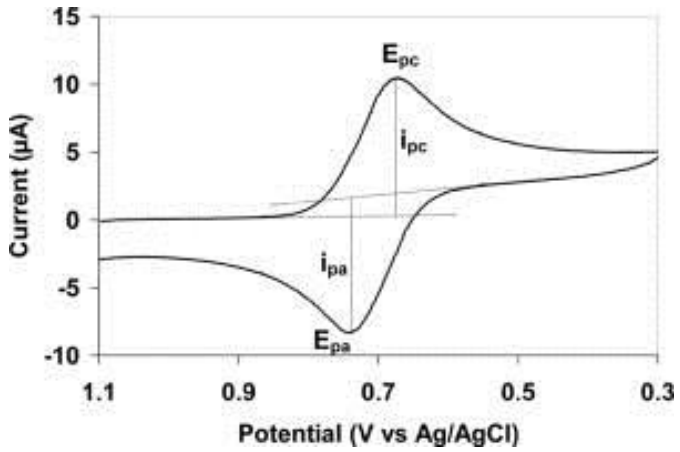

Figure 2.1 Typical cyclic voltammogram for a reversible reaction [5].

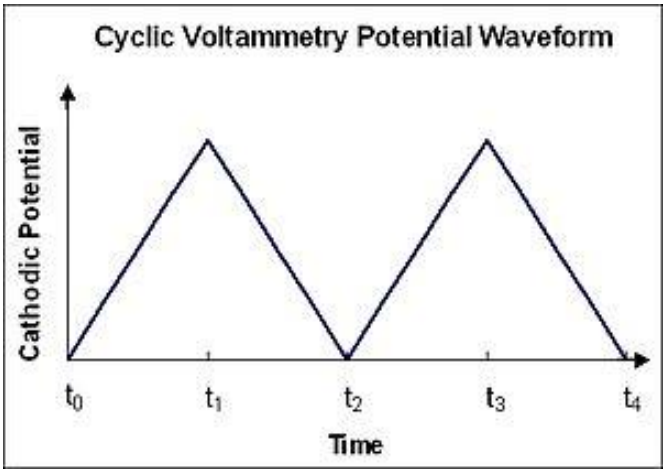

Figure 2.2 Typical cyclic voltammetry waveform [5].

There are two main redox reactions, reversible and irreversible

reaction.Electrochemical reversibility means that the current between cathodic and anodic flow reversibly in broad overpotential region and the electron transfer at the working electrode surface is fast enough. If there is a reversible reaction, it is also called as nernstian reaction because the reversible reaction follows the Nernst equation where E is equilibrium potential, $E^{0'}$ is the formal potential, R is the universal gas constant (8.314J/mol/K), T is the absolute temperature (K), n is the number of electron in the reaction and F is the Faraday's constant (96485C/mol).

$$E = E^{0'} + \frac{RT}{nF} ln \frac{C_0(0,t)}{C_R(0,t)} \qquad (2.1)$$

In reversible reaction, cyclic voltammogram theoretically shows the same peak current of cathodic and anodic reaction and peak potential of both side is a constant versus scan rate (V/s). Additionally, peak current is linearly proportional to root scan rate as shown in Figure 2.3 [6]. However, the irreversible reaction is not satisfied with the Nernst equation. Reverse peak is not shown in cyclic voltammogram and the peak potentials are shifted with various scan rates as shown in Figure 2.4 [6].

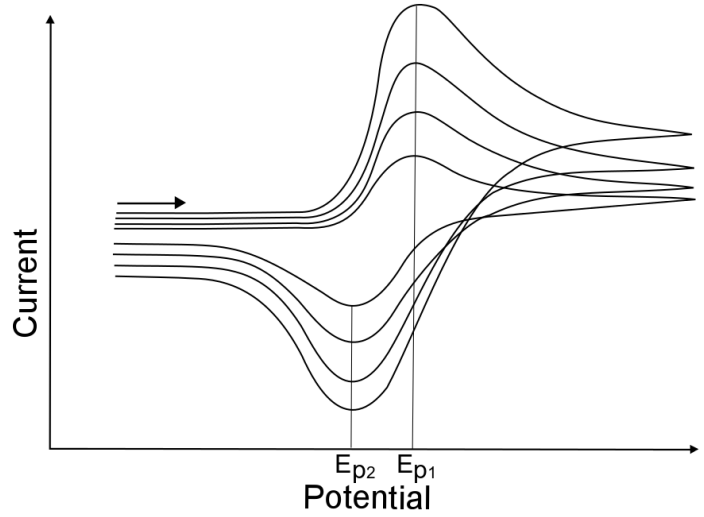

Figure 2.3 Typical cyclic voltammogram of reversible system with various scan rate [6].

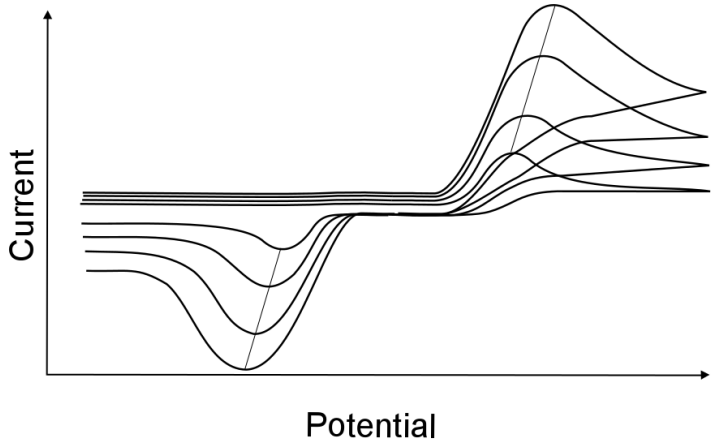

Figure 2.4 Typical cyclic voltammogram of irreversible system with various scan rate [6].

2.2 Electrochemistry modeling code

A time-dependent 1-D simulation of molten salt electrolysis code, REFIN code, was developed by B.G Park as a doctoral dissertation at the Department of Nuclear Engineering of Seoul National University. A time-dependent electrorefining model was developed from the first principle for the kinetic characterization and performance analysis of a multi-component pyroprocessing. This code employed the diffusion layer theory to consider the diffusion and migration in diffusion layer between molten salt and electrode. Butler-Volmer kinetics model at electrode surface was linked with the mass conservation and electric charge neutrality conditions. The results in non-linear partial differential equations for multi component system is converted into a set of ordinary differential equations which is solved by combination of the backward difference scheme and Newton's method.

REFIN has no restriction on the number of energy groups, etc. The solid metal electrode is assumed to have a uniform composition with internal diffusion that is fast enough to homogenize its composition along with non-uniform dissolution or deposition at the interface of metal and molten salt. REFIN also has ability to handle both a solid electrode and a liquid electrode.

The accuracy of simulated results is only as good as the quality of electrochemical and kinetic database for modeled materials. There is also a unique advantage over other existing models developed for

pyroprocessing in this capability of simulating transient phenomena under either electrochemical potential or faradic current control at that time [7].

Chapter 3. Research Goal and Approach

3.1 Research Goal

3.1.1 Main goal

This study is mainly for process development for pyrochemical decontamination of long-living activation products in reactor internals from decommissioning.

3.1.2 Objectives

To process development, basic electrochemical parameters of metallic elements will be studied. Pyrochemical separation process for Ni, Co, Nb will be designed by neutronic activation code and electrochemical process model. Neutronic activation and depletion code will be used for setting the goal of decontamination factors. Electrochemical model will check for decontamination ability and behavior of elements during pyrochemical decontamination process. Pilot-scale unit cell will be designed by 3-D hydrodynamic computer model.

3.2 Research Approach

The dissertation focuses on pyrochemical separation of Nb, Ni, Co from activated stainless steels by electrorefining based on their standard redox

potential differences in LiCl-KCl molten salts.

Overall approach on this dissertation flows as shown in Figure 3.1. There are 4 steps. As a first step, inventory analysis of reactor vessel internals made with type 304 stainless steel is performed to set the goal of decontamination factor for electrorefining process. In second step, it is composed of three main elements that are linear polarization/cyclic voltammetry experiments, electrochemical modeling by REFIN code and lab-scale electrorefining experiments. Basic electrochemical data including apparent reduction potential, diffusion coefficient, exchange current density and charge transfer coefficient are gained from linear polarization/cyclic voltammetry. Using REFIN code and obtained data, electrorefining modeling is performed to check whether process meets the required decontamination factor or not and to study electrochemical behavior of metallic elements during process. After lab-scale electrorefining, composition of deposition on cathode is analyzed by X-Ray Diffraction (XRD) patterns and Inductively Coupled Plasma Mass Spectroscopy (ICP-MS) to calculate decontamination ability and to verify the results from modeling. Pilot-scale conceptual electrorefining unit cell is designed by 3-D hydrodynamic modeling. Some issues from lab-scale electrorefining is studied in this step and new cell design is suggested. Overall process flowsheet including additional refining processes is shown in this step as well. As the last step, cost benefit analysis of decontamination process is conducted. Expected volumetric reduction effect and economical effect of decontamination process is

evaluated.

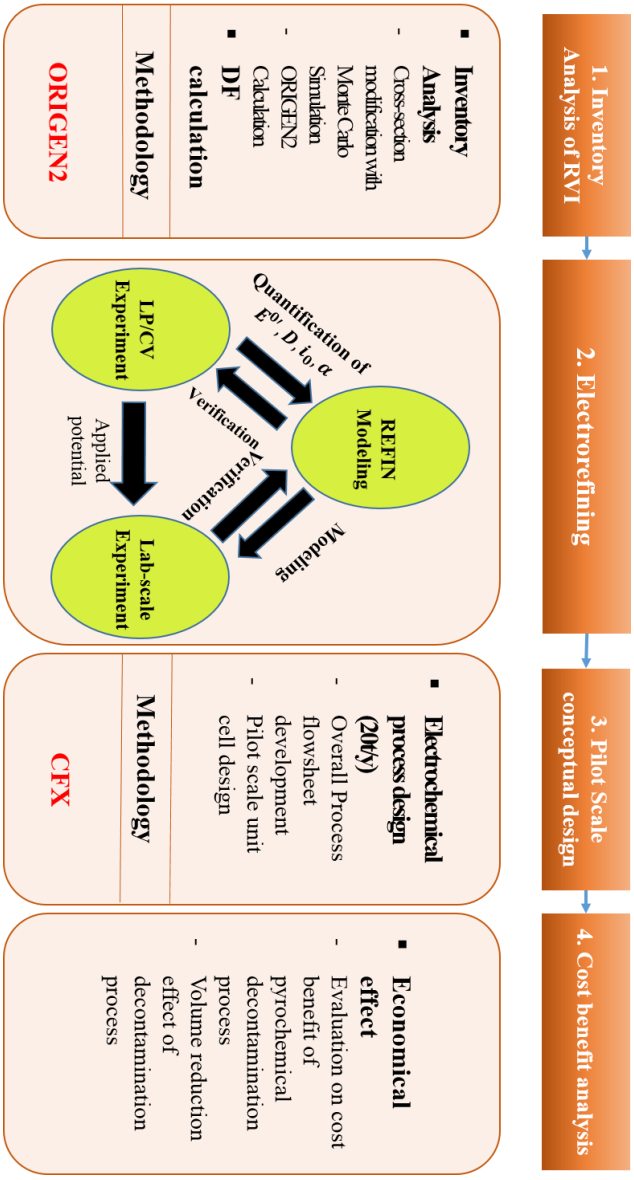

Figure 3.1 4-steps research approach

Chapter 4. Decontamination Requirements for Activated Intermediate Level Waste

4.1 Inventory Analysis of PWR Internals

Reactor vessel internals for PWR such as Kori unit #1 are mainly made of type 304 stainless steel. The main compositions of stainless steel are Cr, Fe, Mn and Ni. Even if minor elements are very small compared to major elements, they still exist to significant levels as shown in Table 4.1 [8]. Inventory analysis of PWR reactor vessel internals (baffle, former, barrel and thermal shield) is performed using ORIGEN-2 code. ORIGEN-2 code is a one-group point depletion code developed by Oak Ridge National Laboratory. Following some assumptions are employed ;

1) PWR 1 unit
2) Pristine type 304 stainless steel with trace elements were irradiated in the maximum neutron flux (1.0E+12 n/cm^2/sec)
3) Effective Full Power Year (EFPY): 32 years (Capacity factor: 80%)
4) Cooling time : 0~100 year

These assumptions are conservative because neutron flux is maximum and there is no temporary shutdown during nuclear power plant operation.

Activation products are produced after 32 EFPY irradiation period. As the cooling period is increased, the radioactivity is reduced as well as shown in Figure 4.1.

Table 4.1 Minor elements of type 304 stainless steel [8].

Nuclides	Composition (wt. %)
Li	1.30E-05
N	4.52E-02
Sc	3.00E-06
Ti	6.00E-02
Co	2.31E-01
Cu	3.08E-01
Zn	4.57E-02
Nb	8.90E-03
Mo	2.60E-01
Ag	2.00E-04
Sb	1.23E-03
Cs	3.00E-05
Ce	3.71E-02
Sm	1.00E-05
Eu	2.00E-06
Lu	8.00E-05
Hf	2.00E-04
Th	1.00E-04

Fe^{55}, Co^{60}, Mn^{54} and Ni^{63} is dominant during few years just after shutdown. But except for Ni^{63}, the radioactivity of Fe^{55}, Co^{60} and Mn^{54} are reduced because their half-lives are very short. This fact also means that they are not important nuclides in the view of long term disposal. For long term disposal, Ni^{63}, Ni^{59}, C^{14}, Nb^{94} and Tc^{99} are important nuclides. They have very long half-lives compared to other nuclides in activated stainless steel. The radioactivity after 15 years of cooling, are expected in the decommissioning point of Kori unit #1, is grossly greater than the criteria of ILW in Korea, as given in Table 1.2.

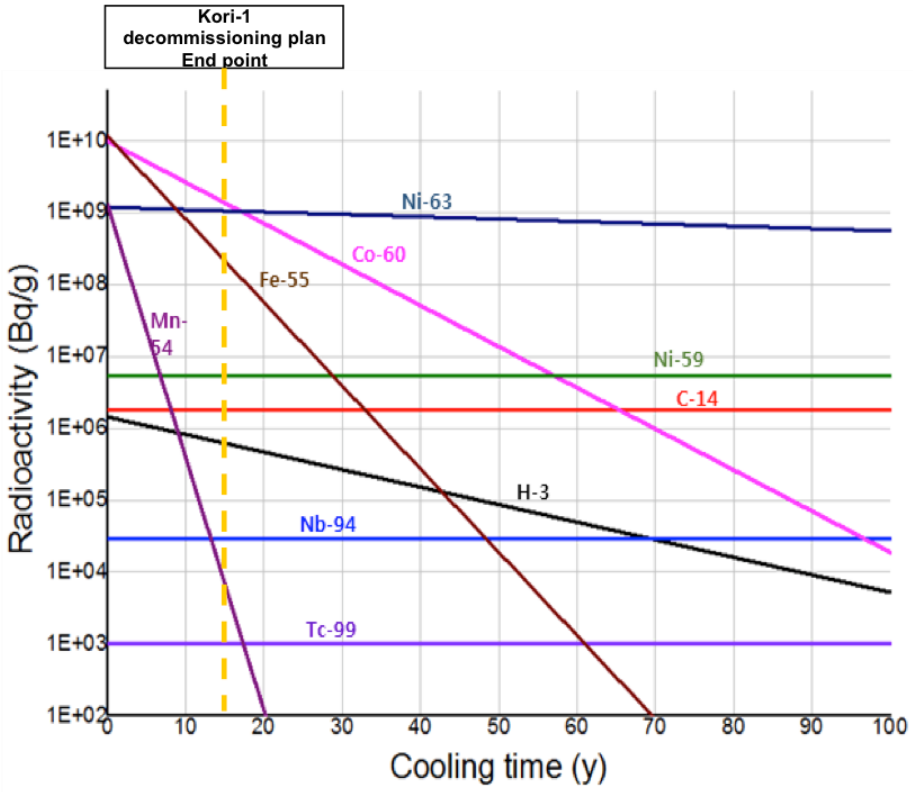

Figure 4.1 Radioactivity of PWR internals after 32 years operation simulated by ORIGEN-2 code.

4.2 Calculation of Decontamination Factor (DF)

This section is aimed at determining decontamination factor (DF) of long living activation products at 15 years cooling time. Radioactivity concentration of C^{14}, Nb^{94}, Ni^{59} and Ni^{63} are greater than Korea Radioactive Waste Agency's acceptance criteria for Gyeongju repository. Decontamination factors required for each nuclide for making ILW into LLW can be calculated by following equation.

Required DF = *Radioactivity (Bq/g) / **Criteria (Bq/g) (4.1)

Table 4.2 Radioactivity of long-living activation products and DF for LLW level for Type 304 stainless steel for Kori unit #1.

Nuclide	*Radioactivity (Bq/g)	**Criteria (Bq/g)	DF (Required)	Half life (Yr)
H^3	6.17E+05	1.11E+06	0.6	12.3
C^{14}	1.83E+06	2.22E+05	8.2	5,730
Nb^{94}	2.88E+04	1.11E+02	259.1	20,000
Co^{60}	1.35E+09	3.70E+07	36.6	5.3
Ni^{59}	5.40E+06	7.40E+04	73.0	76,000
Ni^{63}	1.05E+09	1.11E+07	94.7	100
Tc^{99}	1.03E+03	1.11E+03	0.93	213,000

4.3 Feasibility of Decontamination

Total 20 units of PWR are being operated in Korea and they will be decommissioned at some point. So, it is necessary to study that DF given in Table 4.2 is feasible for applying to 20 units. There is a total activity limit in Gyeongju repository phase 1 for nuclides, H^3(1.37E+15Bq), C^{14}(1.66E+14Bq), Tc^{99}(7.85E+11Bq), Co^{60}(1.03E+15Bq), Ni^{59}(3.78E+13Bq), Ni^{63}(2.71E+15Bq) and Nb^{94}(9.72E+10Bq). When DF is applied to reactor vessel internal of 1 unit, expected radioactivity after decontamination are H^3(6.17E+05Bq/g), C^{14}(2.22E+05Bq/g), Tc^{99}(1.03E+03Bq/g), Co^{60}(3.70E+07Bq/g), Ni^{59}(7.40E+04Bq/g), Ni^{63}(1.11E+07Bq/g) and Nb^{94}(1.11E+02Bq/g). With these radioactivity data, limited quantity of disposable nuclides in phase 1 is very large. Therefore, when DF is also applied to reactor internals of 20 units, all wastes can be disposed as LLW in Gyeongju repository as shown in Table 4.3.

Evaluation on possibility of waste disposal in repository after decontamination for 20 units					
Nuclide	Total Activity limit in Phase 1 (Bq)	Expected radioactivity after decontamination (Bq/g)	Limited Quantity by activity (ton)	Estimated total mass (ton/20 units)	
H^{3}	1.37E+15	6.17E+05	2.22E+03	2.29E-06	• When DF for LLW is achieved and applied for 20 units of PWR currently being operated, all wastes can be disposed as LLW in Gyeongju repository
C^{14}	1.66E+14	2.22E+05	7.48E+02	1.47E-02	
Tc^{99}	7.85E+11	1.03E+03	7.62E+02	2.18E-03	
Co^{60}	1.03E+15	3.70E+07	2.78E+01	4.29E-02	
Ni^{59}	3.78E+13	7.40E+04	5.11E+02	2.56E+00	
Ni^{63}	2.71E+15	1.11E+07	2.44E+02	6.11E-01	
Nb^{94}	9.72E+10	1.11E+02	8.76E+02	5.50E-03	

Figure 4.2 Evaluation on possibility of disposal for reactor internals from 20 units.

Chapter 5. Electrorefining Experiments for Decontamination of Stainless Steel

5.1 Experimental Setup of Cyclic Voltammetry

Electrochemical experimental setup was built in a glove box filled and continually purged with Argon gas (Purity: 99.999 wt. %). Oxygen and moisture contents were maintained lower than 0.1ppm. A proportional-integral-derivative (PID) controller was installed for furnace that were located at the bottom well of the glove box. Electrochemical measurement systems are controlled by a VersaStat3 potentiostat and VersaStudio software.

A LiCl-KCl eutectic salt with purity of 99.99 wt. % and $FeCl_2$ and $NiCl_2$ with purity of 99.99 wt. % and $CoCl_2$ with purity of 99.9 wt. % were supplied from Sigma Aldrich. $CrCl_2$ with purity of 99.9 wt. % were provided from Alfa Aesar. All reagents were open and handled in a glove box. AgCl with the purity of 99.999 wt. % and Tungsten and Ag wires for electrodes were supplied from Sigma Aldrich.

Quartz cell with an inner diameter of 11mm was located in the furnace and three electrodes were put in the quartz cell. Two tungsten wires for working electrode and counter electrode were guided by a quartz tube with an inner diameter of 2mm. The 1cm tip of tungsten wires were dipped in molten salt and contacted area was 0.628cm^2. A Ag wire with

99.99% purity for reference electrode was immersed in Pyrex tube containing LiCl-KCl with 1 wt. % AgCl. The temperature in a quartz cell was kept at 500±1℃ and monitored by a Type-K thermocouple in identical quartz tube attached outer surface of the main cell.

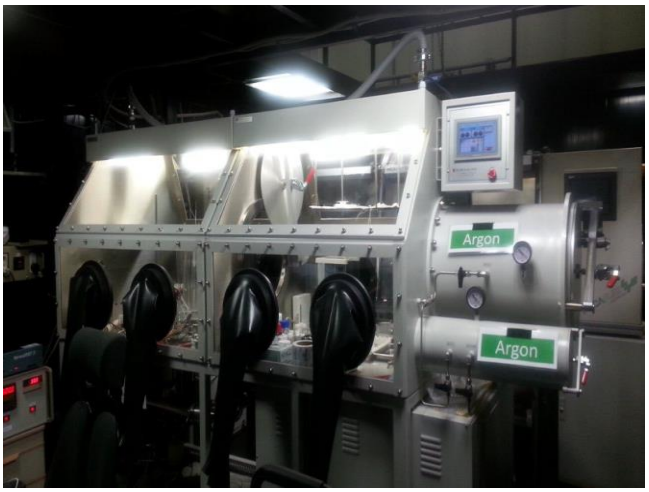

Figure 5.1 Glove box for electrochemical experiments

Figure 5.2 VersaSTAT3 potentiostat and PID heater controller

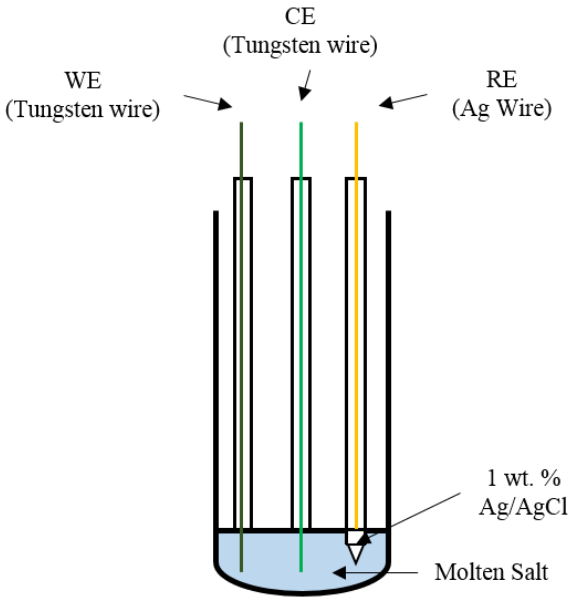

Figure 5.3 Cell design for CV experiments

5.2 Cyclic Voltammetry for Fe, Co, Ni and Cr

Cyclic voltammetry experiments are conducted by test matrix as shown in Table 5.1. Fe ions have various and relatively high concentration experiments. Fe ion is expected to be abundant during electrorefining process. However, Co, Ni and Cr ions are relatively low concentrated in molten salt.

Table 5.1 Experiments test matrix for CV

Reaction	Temperature	Concentration	Scan rate
Fe/Fe^{2+}	773 K	1 wt. %	- 30 mV/s - 50 mV/s - 100 mV/s - 150 mV/s - 200 mV/s
		3 wt. %	
		5 wt. %	
Co/Co^{2+}		0.1 wt. %	
Ni/Ni^{2+}		0.1 wt. %	
Cr/Cr^{2+}		1.2 wt. %	

Before CV experiments of Fe, Co, Ni and Cr, CV experiment of pure LiCl-KCl eutectic molten salt was conducted to check the background condition of molten salt. Cyclic voltammogram of LiCl-KCl is shown in Figure 5.4. It reveals that there is very small background current density which has no big effect on other results.

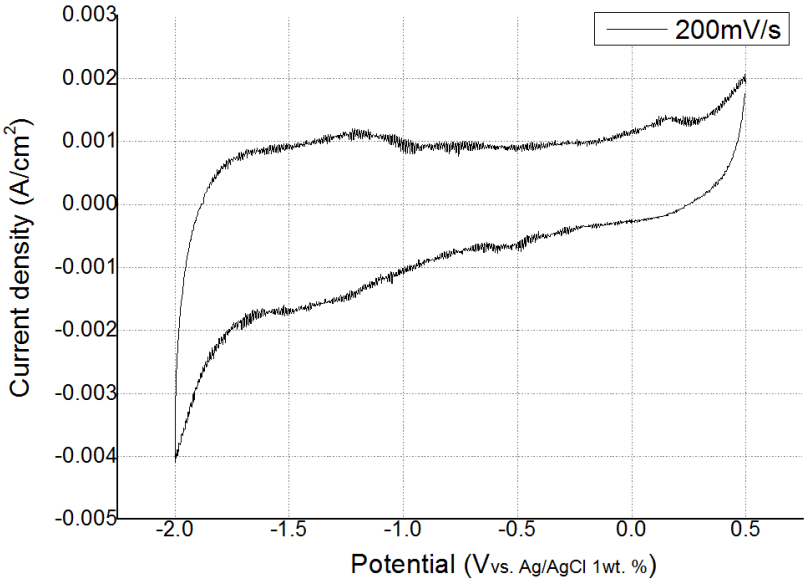

Figure 5.4 Cyclic voltammogram of eutectic LiCl-KCl molten salt.

After that, the results of all cyclic voltammetry are presentedin Figures 5.5~5.10. In agreement with earlier studies [9,10],all cases except for Cr case have a simple redox peak pair. Fe, Co and Ni have single soluble state in LiCl-KCl in given scan range. However, Cr shows two oxidation states in the scan range. Therefore, redox reaction of Cr^{2+} and Cr^{3+} can be ignored to consider as shown in Figure 5.10. But for Fe cases, an interesting potential range will be formed only within -0.6V~0V (vs. 1 wt. % Ag/AgCl).

Anodic peak potentials in Fe cases are formed between -0.25V and -0.15V (vs. 1 wt. % Ag/AgCl). Other cases form in more positive region. That difference will make selective oxidation from anode.

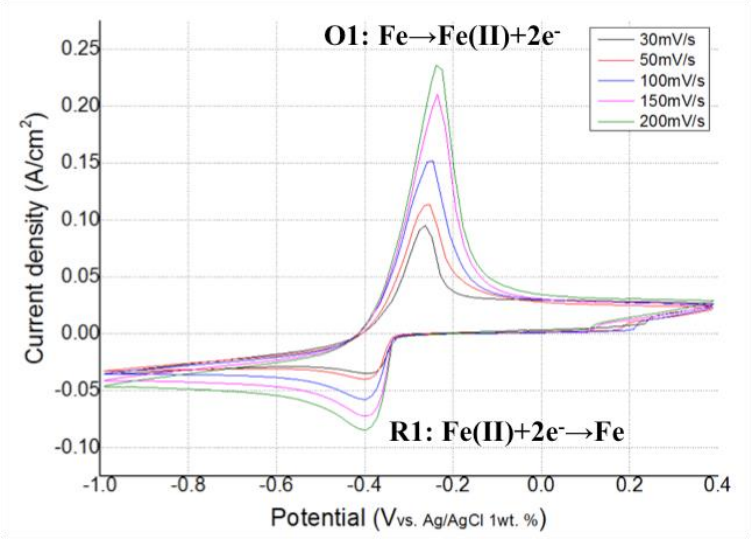

Figure 5.5 Cyclic voltammogram according to scan rate for the scan range from −1.0V to 0.4V (vs. 1wt. % Ag/AgCl) in 773K, LiCl-KCl-$FeCl_2$(1 wt. %)

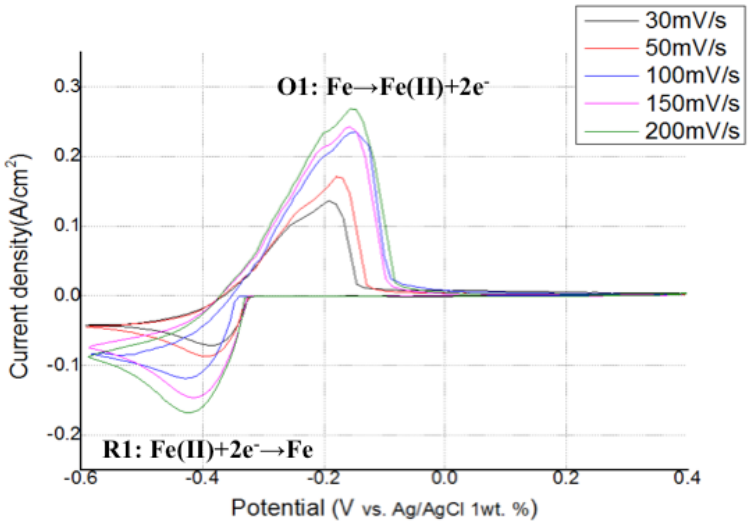

Figure 5.6 Cyclic voltammogram according to scan rate for the scan range from −0.6V to 0.4V (vs. 1wt. % Ag/AgCl) in 773K, LiCl-KCl-$FeCl_2$(3 wt. %)

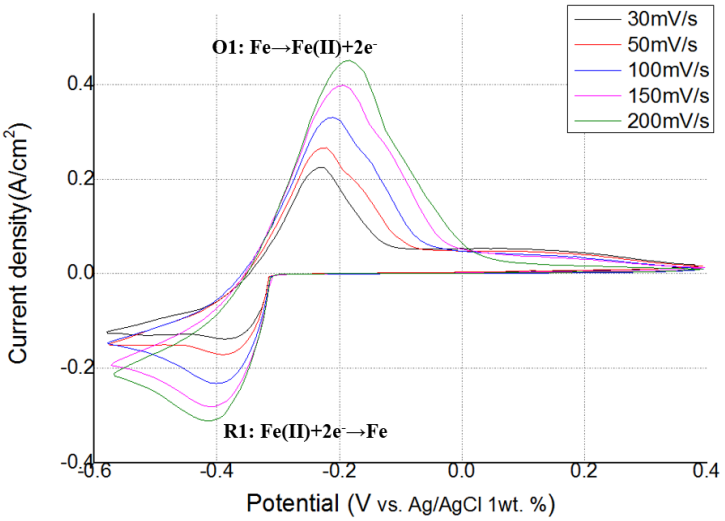

Figure 5.7 Cyclic voltammogram according to scan rate for the scan range from −0.6V to 0.4V (vs. 1wt. % Ag/AgCl) in 773K, LiCl-KCl-$FeCl_2$(5 wt. %)

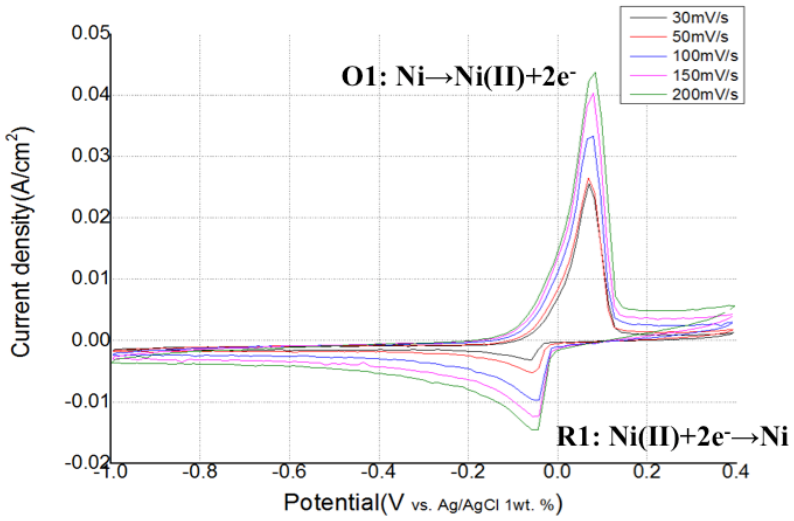

Figure 5.8 Cyclic voltammogram according to scan rate for the scan range from −1.0V to 0.4V (vs. 1wt. % Ag/AgCl) in 773K, LiCl-KCl-$NiCl_2$(0.1 wt. %)

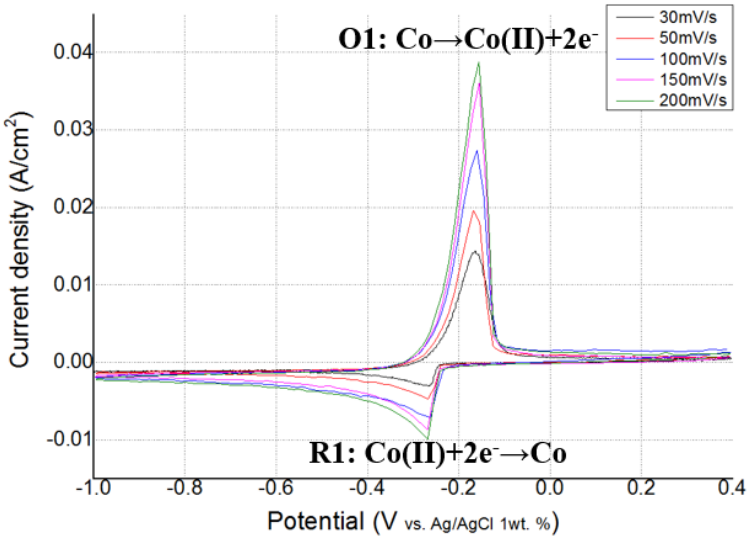

Figure 5.9 Cyclic voltammogram according to scan rate for the scan range from −1.0V to 0.4V (vs. 1wt. % Ag/AgCl) in 773K, LiCl-KCl-$CoCl_2$(0.1 wt. %)

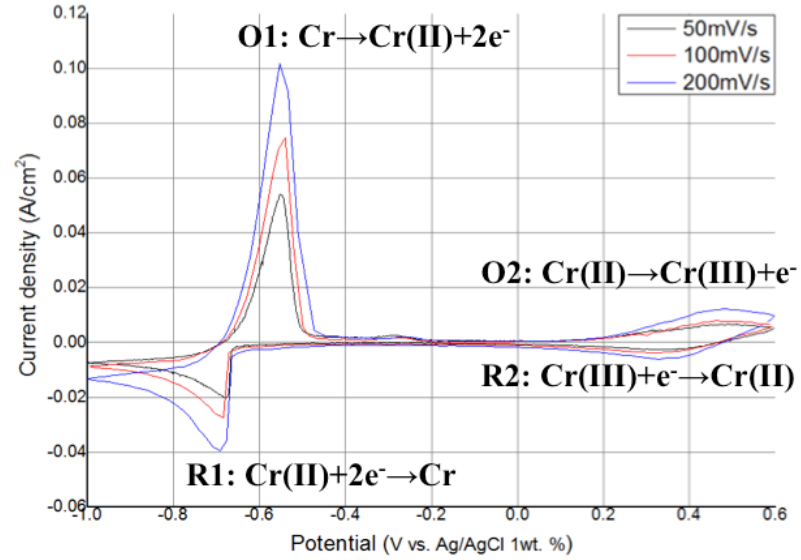

Figure 5.10 Cyclic voltammogram according to scan rate for the scan range from −1.0V to 0.6V (vs. 1wt. % Ag/AgCl) in 773K, LiCl-KCl-$CrCl_2$(1.2 wt. %)

From cyclic voltammetry results, apparent reduction potential of Fe^{2+}, Co^{2+}, Ni^{2+} and Cr^{2+} in LiCl-KCl at 773K can be estimatedusing following Nernst equation:

$$E^{0'} = E_p - \frac{RT}{nF} lnX_{M^{n+}} - 0.854\frac{RT}{nF} + E^0_{AgCl} + \frac{RT}{F} lnX_{AgCl} \quad (5.1)$$

where $E^{0'}$ is the apparent reduction potential (V), E_p isthe peak potential (V), R is the gas constant (8.314J/mol-K), T is the temperature (K), n is the number ofelectrons, F is the Faraday constant (96,485 C/mol), andX_{Mn+} is the mole fraction of M^{n+}. The standardreduction potential of Ag (-0.853 V vs. Cl_2/Cl^- reportedby Iizuka et al.[11]) was used to convert the measuredpotentials from Ag/AgCl reference to Cl_2/Cl^-.

The diffusion coefficients of Fe^{2+}, Co^{2+}, Ni^{2+} and Cr^{2+} in LiCl-KCl at 773K can be also assessed using cathodic peak current variation with the square root of scan rates. From CV, they are calculated based on the Berzins-Delahay equation for a reversible electrodeposition.

$$i_p = 1.082nFAC\sqrt{\frac{nFDv}{RT\pi}} \quad (5.2)$$

where i_p is the peak current (A), A is the electrode area(cm^2), D is diffusion coefficient (cm^2/s), and v is scanrate (V/s).

The overall results from above calculations are summarized in Table 5.2.

Table 5.2 Apparent reduction potential and diffusion coefficients from cyclic voltammetry experiments.

	Concentration (wt. %)	E (V vs. 1 wt.% Ag/AgCl)	D (cm^2/s)
$FeCl_2$	1	-0.225	4.70E-10
	3	-0.262	2.11E-09
	5	-0.278	7.72E-09
$CoCl_2$	0.1	-0.017	5.64E-10
$NiCl_2$	0.1	0.198	9.46E-10
$CrCl_2$	1.2	-0.100	9.86E-09

5.3 Exchange Current Density Determination by Linear Polarization Method

The exchange current density and the transfer coefficient are important electrochemical parameters for evaluating the electrorefining process. However, only a few studies have been performed to investigate both parameters of actinides for pyroprocessing development. Even fewer studies on metal elements exist.

Tafel method, linear polarization method and electrochemical impedance spectroscopy are generally used to investigate the exchange current density and the charge transfer coefficient. Among these methods, Tafel graph produced by linear polarization method is used in this dissertation.

Butler-Volmer equation is describing the charge transfer kinetics of soluble-insoluble process.

$$i = i_0 \left[exp\left(\frac{\alpha nF}{RT}\eta\right) - exp\left(-\frac{(1-\alpha)nF}{RT}\eta\right)\right] \quad (5.3)$$

where i is the current density (A/cm^2), i_0 is theexchange current density (A/cm^2), α is the chargetransfer coefficient and η is the overpotential (V).

For sufficient overpotential region, Eq.5.3 can be simplified to

$$\ln(i) = ln(i_0) - \frac{\alpha nF}{RT}\eta \quad (5.4)$$

When linear fitting is applied to sufficient overpotential region, the exchange current density and the charge transfer coefficient can be derived from the slope and intersection of linear fitting. Tafel plots of all cases are shown in Figure from 5.11 to 5.16. Derived exchange current density and charge transfer coefficient are summarized in Table 5.3.

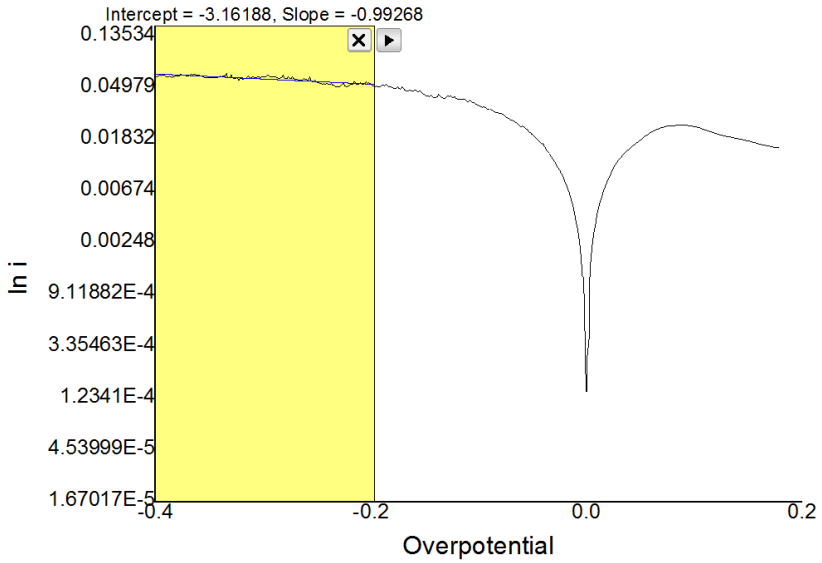

Figure 5.11 Tafel plot of Fe^{2+} with 1 wt. % concentration in LiCl-KCl at 773K.

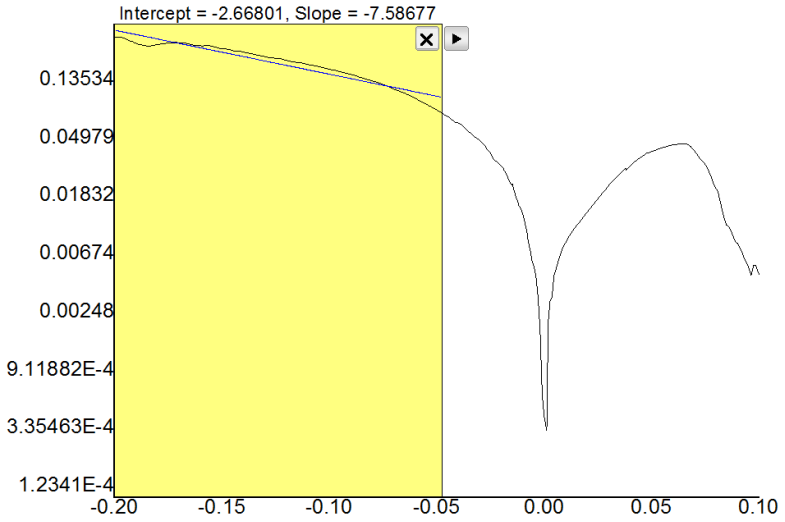

Figure 5.12 Tafel plot of Fe^{2+} with 3 wt. % concentration in LiCl-KCl at 773K.

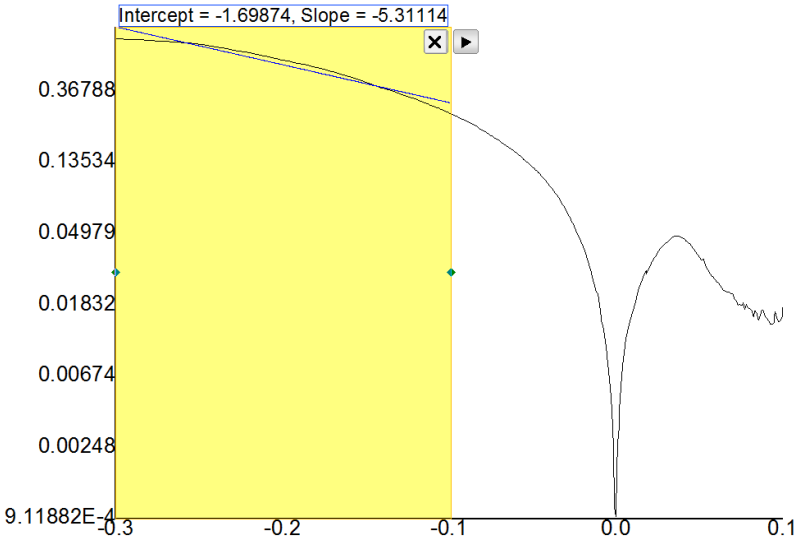

Figure 5.13 Tafel plot of Fe^{2+} with 5 wt. % concentration in LiCl-KCl at 773K.

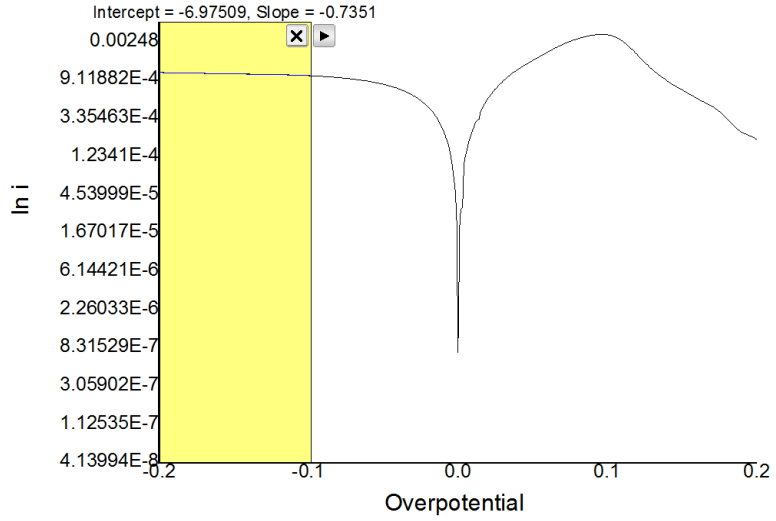

Figure 5.14 Tafel plot of Co^{2+} with 0.1 wt. % concentration in LiCl-KCl at 773K.

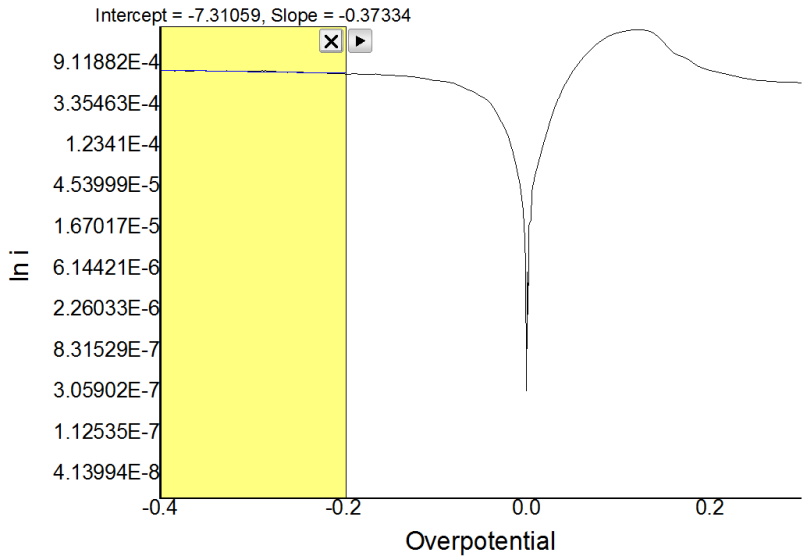

Figure 5.15 Tafel plot of Ni^{2+} with 1 wt. % concentration in LiCl-KCl at 773K.

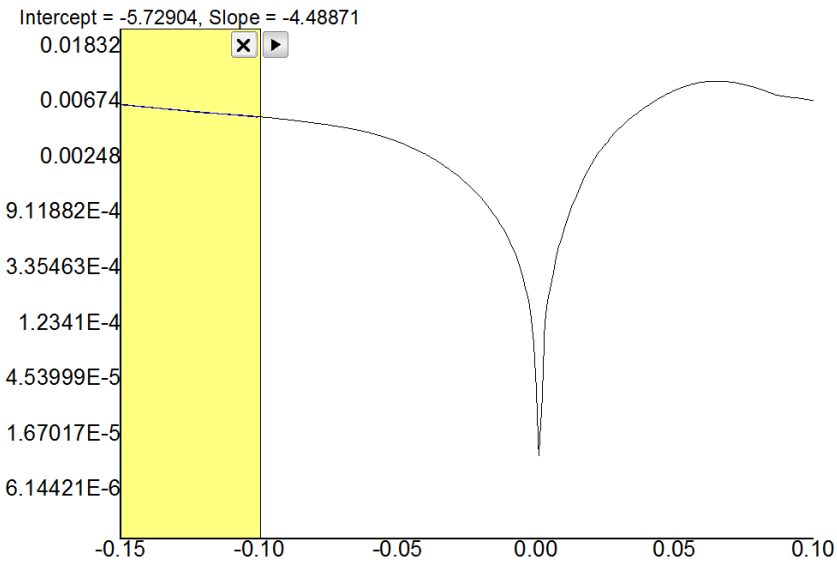

Figure 5.16 Tafel plot of Cr^{2+} with 1.2 wt. % concentration in LiCl-KCl at 773K.

Table 5.3 Exchange current density and charge transfer coefficient of Fe^{2+}, Co^{2+}, Ni^{2+} and Cr^{2+}.

	Concentration (wt. %)	I (A/cm^2)	α
$FeCl_2$	1	4.23E-02	0.033
	3	6.93E-02	0.253
	5	1.87E-01	0.177
$CoCl_2$	0.1	9.35E-04	0.024
$NiCl_2$	0.1	1.06E-03	0.012
$CrCl_2$	1.2	3.25E-03	0.149

5.4 1-D Electrorefining modeling

Preliminary electrorefining modeling of type 304 stainless steel is performed by REFIN code, 1-D time-dependent simulation code of molten salt electrolysis. There are some assumptions.

1) $Nb(III) + 3e^- \rightarrow Nb$: Considered
2) Nb_xCl_y formation : Ignored
3) Reduction of other ions : Considered as one step reaction

Cell design and basic parameters for 1-D electrorefining modeling is shown as Figure 5.17 and Table 5.4.

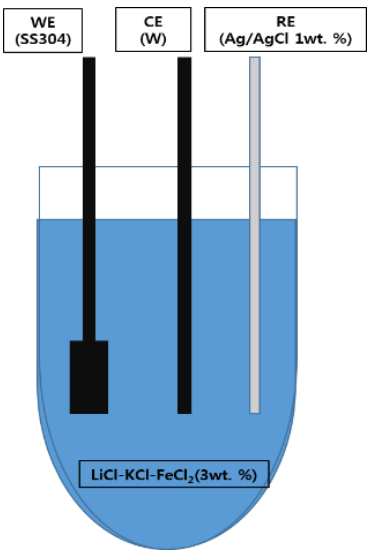

Figure 5.17 Cell design for preliminary electrorefining modeling

Table 5.4 Condition of preliminary electrorefining modeling

	Mass (g)	Area (cm^2)	Volume (cm^3)
Anode (Fresh type 304 stainless steel)	5	4.5	0.625
Cathode	-	0.95	-
Molten salt (LiCl-KCl-3wt. % $FeCl_2$)	40	-	24.69

The results are shown in the form of time dependent changing of deposited mass on cathode. Calculating DF with the ratio of initial compositions on anode and deposited mass on cathode, the summarized results are shown in Figure 5.18. the compared results with required DF is also shown as Table 5.5. DF are decreasing when the recovery of Fe is increasing. Additionally, DFs of Co and Nb are greater than the required DF to be LLW, however, DF of Ni is stayed under the required DF. This fact shows that two step electrorefining processes are needed to meet required DF.

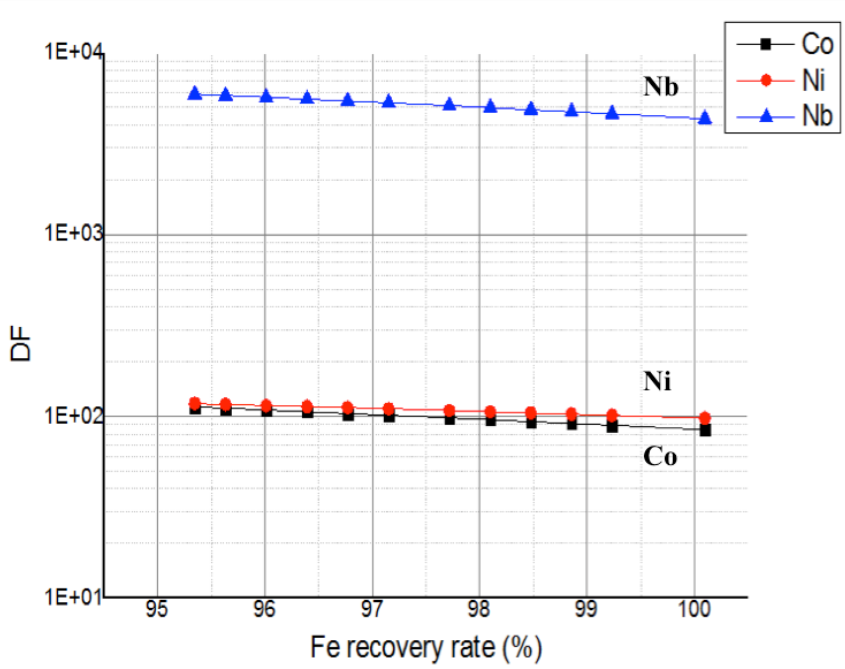

Figure 5.18 DF results for Co, Ni and Nb versus Fe recovery rate (%).

Table 5.5 Comparison of required DF and preliminary modeling results.

DF		Nb	Co	Ni
Required	LLW	2.59E+02	3.66E+01	9.47E+01
Fe recovery	99%	4.39E+03	1.01E+02	8.94E+01
	99.9%	4.09E+03	9.71E+01	8.40E+01
	99.99%	4.07E+03	9.67E+01	8.35E+01

5.5 Experimental Setup of Electrorefining

Experimental setup of electrorefining such as the equipment, software, operating temperature and conditions in a glove box is equal to cyclic voltammetry experiments. LiCl-KCl molten salt were used for all experiments at 500℃.

A LiCl-KCl eutectic salt with purity of 99.99 wt. % and $FeCl_2$ with purity of 99.99 wt. % were supplied from Sigma Aldrich. All reagents were open and handled in a glove box. AgCl with the purity of 99.999 wt. % and Ag wires for reference electrode were supplied from Sigma Aldrich.

Quartz cell with an inner diameter of 27mm and flat bottom face was located in the furnace. A tungsten rod with a diameter of 3.175 mm and purity of 99.95 wt. % from Alfa Aesar was used for counter electrode. The 2.5cm tip of tungsten rod was dipped in molten salt and contacted area was 2.57cm^2. Pristine type 304 stainless steel rod made by POSCO Co. with a diameter of 5mm was used as anode and the composition difference between pristine metals and activated metals is small enough. The 2.5cm tip of stainless steel rod was also dipped in molten salt and contacted area was 4.121cm^2. A Ag wire with 99.99% purity for reference electrode was immersed in Pyrex tube containing LiCl-KCl with 1 wt. % AgCl.Anhydrous LiCl-KCl eutectic salt and $FeCl_2$ from the same source above was used as electrolyte. The concentration of $FeCl_2$ in LiCl-KCl was kept as 3 wt. %.

A comparison result of fresh stainless steel and irradiated steel

compositions are shown as Table 5.6. Details of experimental cell design is presented in Figure 5.19. In Figure 5.19, deposition point on cathode, detached depositions from cathode into basket, bulk salt and detached metals from anode into basket is marked with following numbers.

Table 5.6 Comparison of pristine stainless steel and activated steel compositions from ORIGEN-2 results.

	Pristine Type 304 stainless steel(%)	Activated Type 304 stainless steel composition(%) from ORIGEN-2 results
Cr	18-20	20.34
Ni	8-10.5	10.78
Mn	2	1.75
Co	0.2	0.12
Nb	1.20E-03	8.79E-03
Fe	Balanced (~65.35)	66.69

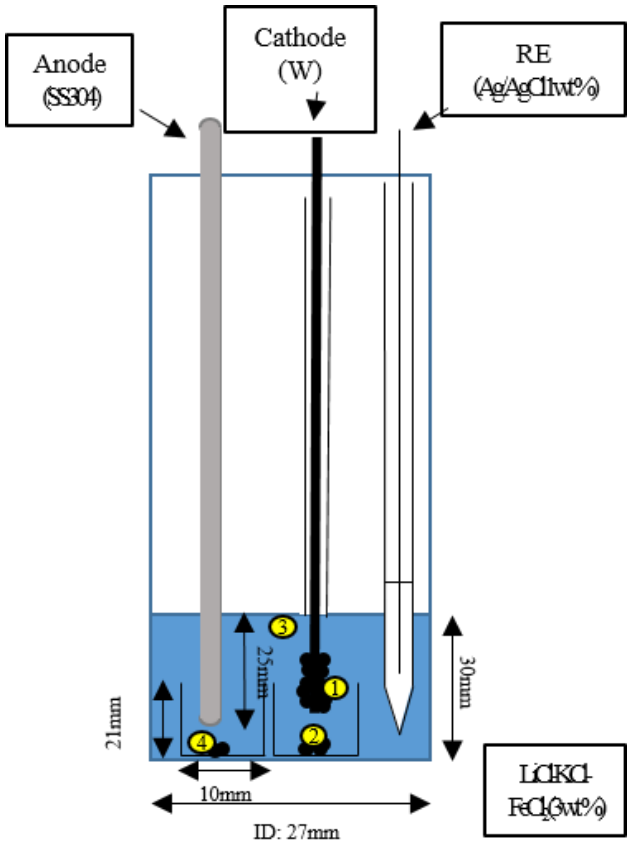

Figure 5.19 Cell schematic for electrorefining experiments.

5.6 Electrorefining of Stainless Steel

Lab-scale electrorefining of stainless steel is performed three times with different applied potential on anode as shown in Table 5.7. Objective of electrorefining is to recover main elements such as Fe, Cr remaining Nb, Co and Ni at anode or anode basket. It is controlled by dissolving process adjusting anode potential.

Since open circuit voltage in the cell was measured to be about -0.28V ~ -0.3V (vs. 1wt. % Ag/AgCl) in the LiCl-KCl-$FeCl_2$ (3 wt. %) with type 304 stainless steel as anode, applied potential range was set from -0.2V to 0V (vs. 1wt. % Ag/AgCl). Current densities of three cases are measured during experiments. When applied potential on anode is increased, current also increase. It can be analyzed from CV results. In 0V (vs. 1wt. % Ag/AgCl) case, increasing current density is shown in Figure 5.20. that is reason why the surface of electrode is increased and the reaction rate is increased as follow.

Depositions at the cathode at -0.2V, -0.1V and 0V (vs. 1 wt. % Ag/AgCl) of the applied anode potential,molten salts, anode basket andcathode basket for -0.2V (vs. 1 wt. % Ag/AgCl) of the applied potential are shown in Figure 5.21.

The ICP-MS results of all metal deposits and molten salt in cell are presented in Figure 5.22 and XRD patterns are also shown in Figure 5.23 ~ 5.25. Marked peak in XRD spectra means that Fe metal was deposited on cathode in all cases and other peaks are produced from LiCl-KCl as

background. Detectability of ICP-MS is reported as 1ppb for Nb, Co, Ni.

Table 5.7 Test matrix of lab-scale electrorefining experiments for type 304 stainless steel at 500℃.

Case	Type 304 stainless steel mass	Applied potential [vs. 1 wt. % Ag/AgCl]
#1	5g	-0.2V @ Anode
#2	5g	-0.1V @ Anode
#3	5g	0V @ Anode

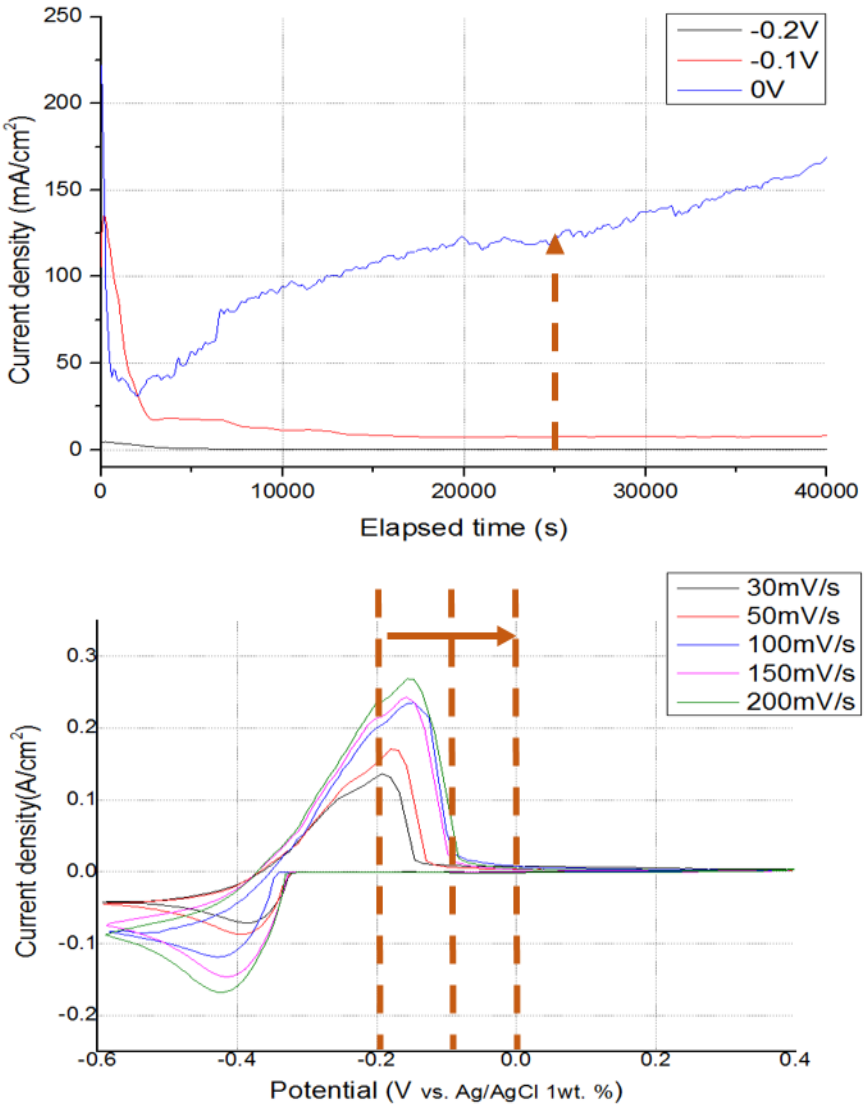

Figure 5.20 Analysis of current density during electrorefining experiments type 304 stainless steel.

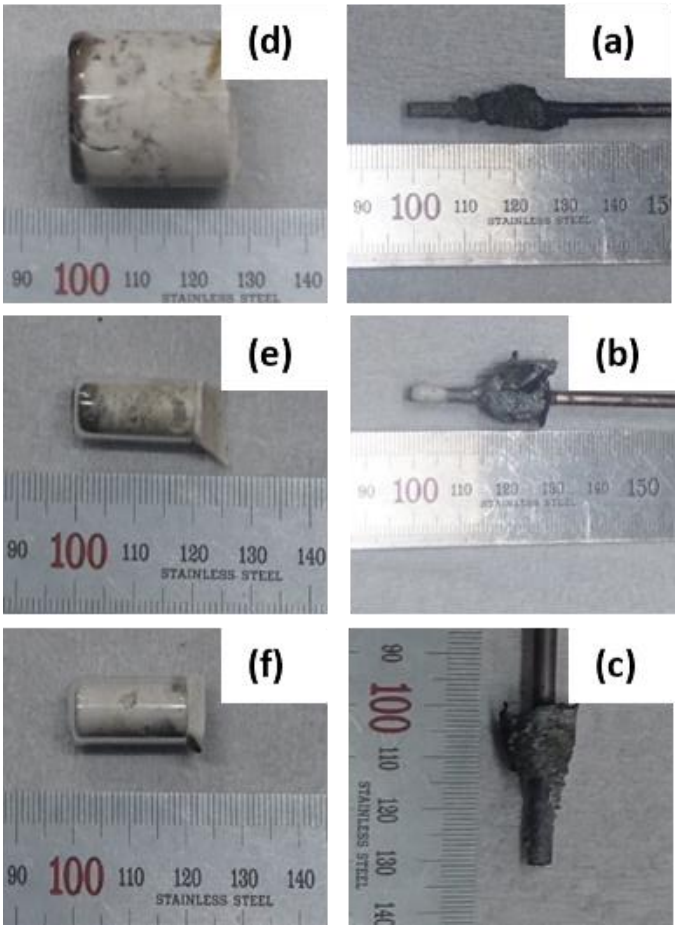

Figure 5.21 Depositions at the cathode at (a) −0.2V, (b) −0.1V and (c) 0V (vs. 1 wt. % Ag/AgCl) of the applied anode potential. (d) Molten salts, (e) Anode basket, (f) Cathode basket for −0.2V (vs. 1 wt. % Ag/AgCl) of the applied potential for electrorefining experiments with type 304 stainless steel.

[Unit : ppm]

① Cathode

Element	Anode -0.2V	Anode - 0.1V	Anode 0V
Nb	N/D	N/D	N/D
Co	110.7	139.2	175.6
Ni	984.9	2106.1	3254.9

② Cathode basket

Element	Anode -0.2V	Anode - 0.1V	Anode 0V
Nb	N/D	N/D	N/D
Co	0.7	2.3	0.8
Ni	3.6	19.6	73.7

[Background in MS : Nb, Co = 0 ppm, Ni = 3.05 ppm]

③ Bulk Molten Salt

Element	Anode -0.2V	Anode - 0.1V	Anode 0V
Nb	N/D	N/D	N/D
Co	0.03	0.4	0.3
Ni	0.2	2.8	2.2

④ Anode basket

Element	Anode -0.2V	Anode - 0.1V	Anode 0V
Nb	N/D	N/D	N/D
Co	0.3	2.0	24.6
Ni	0.5	70.0	361.2

Figure 5.22 ICP-MS results of the molten salt and the deposition at the cathode for electrorefining experiments with type 304 stainless steel.

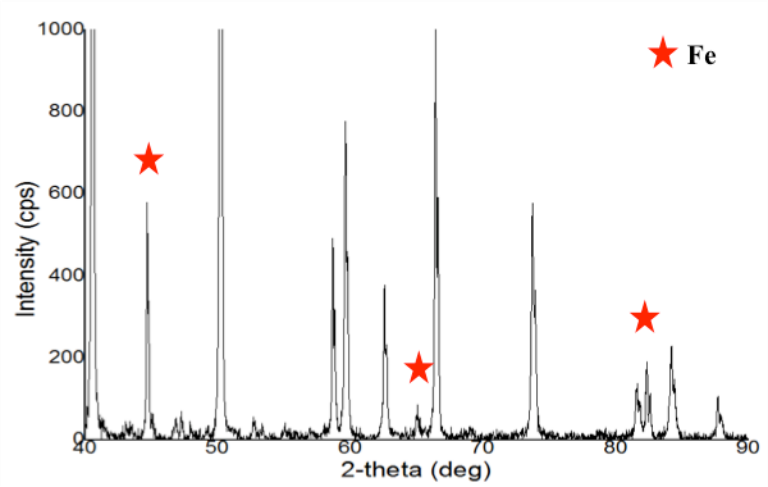

Figure 5.23 XRD pattern of deposition on cathode in Case #1 for electrorefining experiments with type 304 stainless steel.

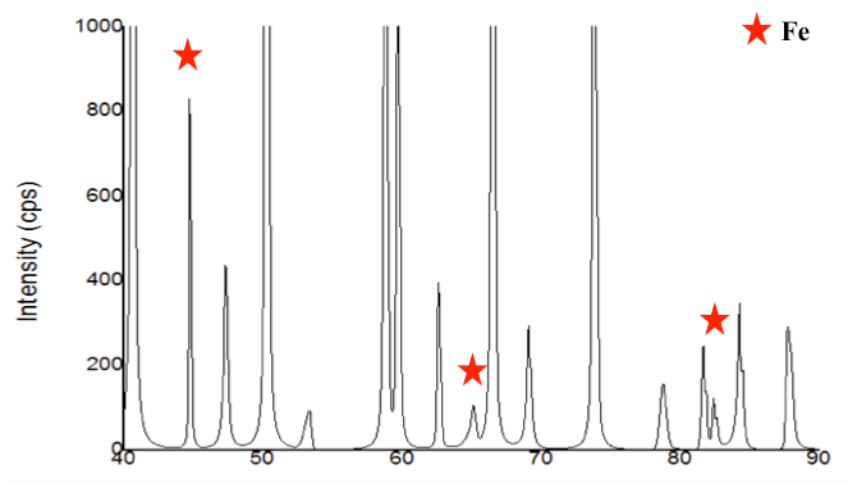

Figure 5.24 XRD pattern of deposition on cathode in Case #2 for electrorefining experiments with type 304 stainless steel.

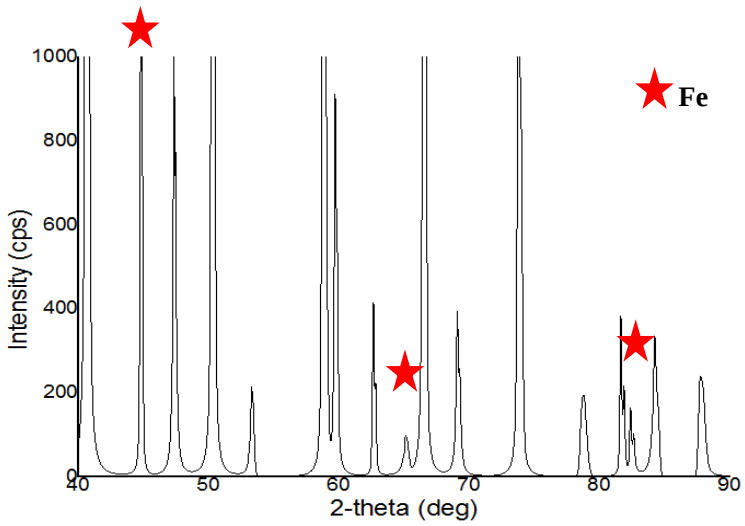

Figure 5.25 XRD pattern of deposition on cathode in Case #3 for electrorefining experiments with type 304 stainless steel.

From ICP-MS results, achieved DF for each elements are summarized in Table 5.8. It shows that DF for Nb is large enough in all cases and DFs for Co, Ni are smaller than required DF. It implies that two-step electrorefining process should be required as shown in Table 5.9.

Table 5.8 Achieved DF for each elements from ICP-MS results.

Element	Required DF	Case #1	Case #2	Case #3	Average
Nb	259.1	∞	∞	∞	∞
Co	36.6	20.9	16.6	13.2	16.9
Ni	94.7	93.9	43.9	28.4	55.4

Table 5.9 Waste level of each elements with n^{th} step of electrorefining.

Element	Before electrorefining	Electrorefining Step 1	Electrorefining Step 2	Expected DF after Step 2
Nb	ILW	LLW	LLW	∞
Co	ILW	ILW	LLW	285.6
Ni	ILW	ILW	LLW	3069.2

Chapter 6. Pilot-Scale Conceptual Design

6.1 Overall Pyrochemical Decontamination Process Flowsheet

From the lab-scale electrorefining results from Chapter 5, two-step electrorefining processes are needed to meet requirements of DFs. Based on this conclusion, overall pyrochemical decontamination process flowsheet is developed in Chapter 6.

H^3 will be evaporated in form of H_2 from anode due to the high temperature of process. It will be trapped by SDBC filter (KAERI/HTR-3047/2005) such as already being used in the off-gas treatment process of pyroprocessing. After 2^{nd} stage of electrorefining, deposited metal scrap can be gained from cathode. So, ingot making process will be required to make a shape for easy disposal to Gyeongju LILW repository. Remainders of anode basket and anode will be Nb, Ni, Co and C. Those will be sent to ILW vitrification process that vitrify ILW waste to be stored in interim storage. Additional salt purification is also demanded for recycling of pure LiCl-KCl as electrolyte of electrorefining.

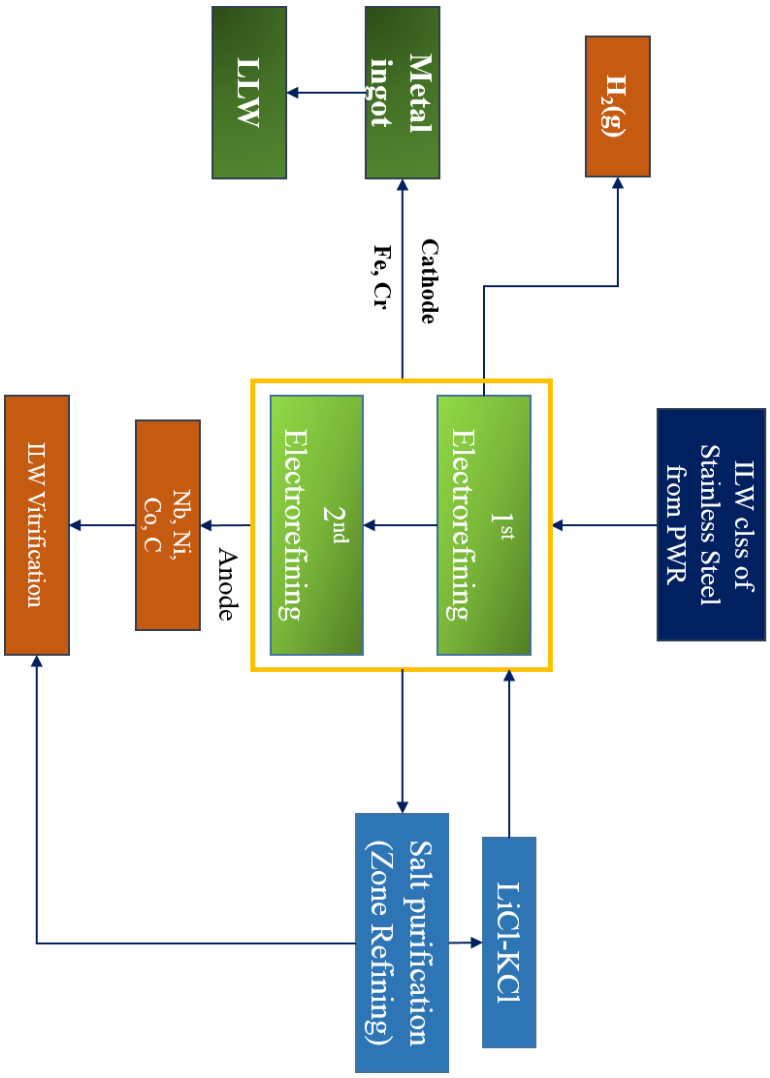

Figure 6.1 Overall pyrochemical decontamination process flowsheet.

6.2 Issues for Cell design

Some issues arise from lab-scale electrorefining process within cell design. Major problem is caused by the existence of basket for collecting detached particles. The basket introduced IR drop while particle products are better separated. The effect of issues will be investigated CFX program, 3-D hydrodynamic computer model.

6.2.1 IR drop

Baskets for both electrodes intervene current flow in a cell so that they make long diffusion path of ions in eutectic LiCl-KCl molten salt. To make it short, baskets are revised to include 16 holes per basket, as shown in Figure 6.2.

There are several assumptions for simulation :

1) Rotating speed of Anode and Cathode: 50 rpm (referenced by Mark-IV electrorefiner)
2) Current density (100mA/cm^2) was referenced from 0V (vs. 1 wt. % Ag/AgCl) case.
3) Anode potential : 0V vs. 1 wt. % Ag/AgCl

The lowest electrical potential on cathode is reduced from -2.87E-01V to -1.35E-01V. The IR drop between anode and cathode become smaller by more than 2 times, as shown in Figure 6.2.

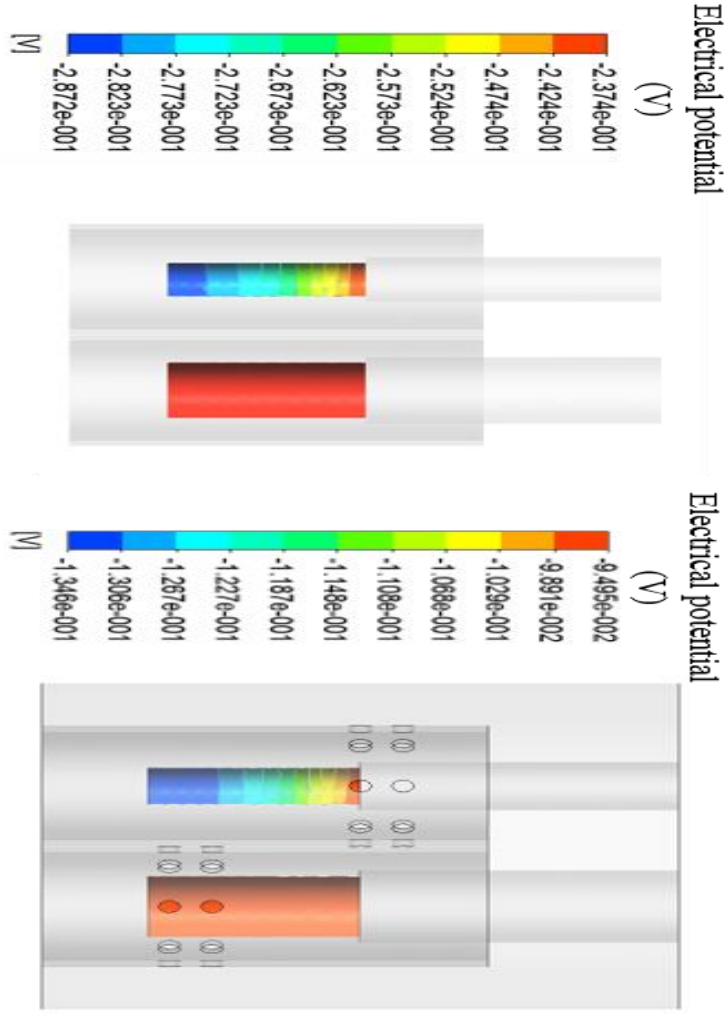

Figure 6.2 Comparison of IR drop simulation by CFX.

6.2.2 Particle tracking

If the revised design with 16 holes is applied, there can be a new problem with particles moving in molten salt due to the turbulent flow caused by rotating electrodes. To identify the possibility of escape, particle tracking simulation is performed.

There are several assumptions for simulation :

1) Rotating speed: 50 rpm (referenced by Mark-IV electrorefiner)
2) A diameter of particle was set as 1.0E-06m.
3) Tracking time of particle was set as 2000sec.

Velocity around electrodes and particle tracking path are shown in Figure 6.3. In original cell design case, there was no escape of particle from basket. Particle is rarely coming out from the anode basket. However, no intrusion of particle into cathode basket is observed in simulation.

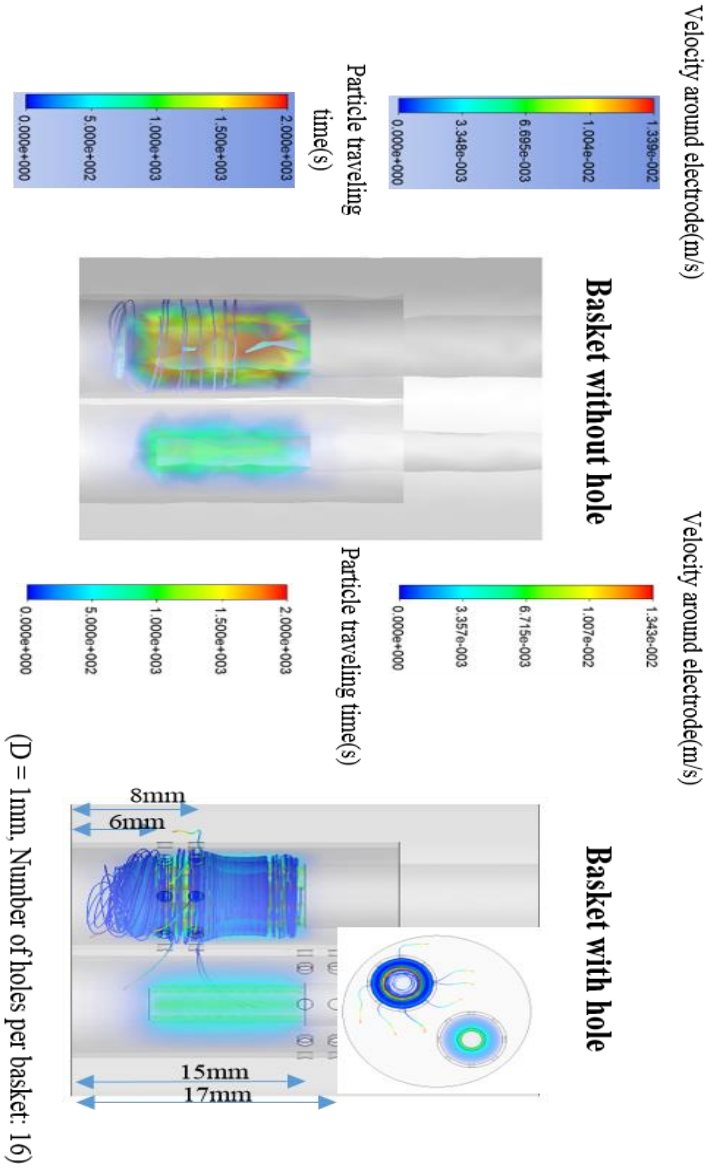

Figure 6.3 Identification of particle escape problem with the revised design by CFX.

6.3 Unit Cell Design

Unit cell design for pilot-scale electrorefiner is devised by the results from Section 6.2 with some assumptions.

1) The goal of throughput : 20 ton/y
2) Working day : 200 days per year
3) Working hour : 24 hours per day

If the electrode with a diameter of 50cm and height of 50cm is set, 4 unit cells in Figure 6.4 need to be constructed in parallel.

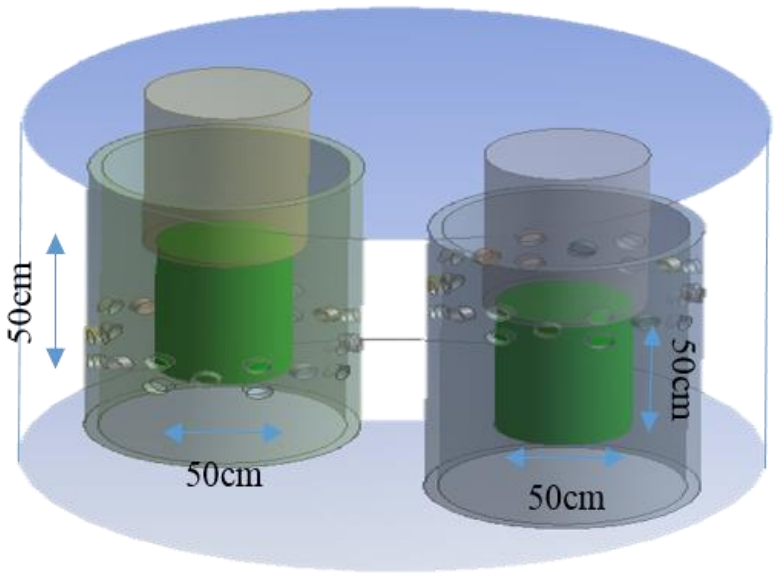

Figure 6.4 Unit cell design for pilot-scale electrorefiner

6.4 Cost Benefit Analysis

Economical benefits on the disposal are investigated in this section. LL-ILW waste disposal costs 273.5 million won per drum which was reported by Sweden SKB report 2010. LLW waste disposal costs 13.73 million won per drum in Korea [12]. The costs for disposal economically reduce about a twentieth. If all long-living activation products are separated from wastes, mass decreases about a seventh.

Figure 6.5 Economical and volumetric effects of decontamination process.

There are assumptions for quantification of both effects :

1) Vitrification waste density : 2,230kg/m^3
2) Fe metal density : 7,680kg/m^3
3) Packing Factor: 0.8

Reduced disposal cost for PWR 20 units =

$$ILW\ \ disposal\ \ cost\ \ before\ \ decontamination -$$
$$\{Vitrified\ \ ILW\ \ disposal\ \ cost +$$
$$LLW\ \ disposal\ \ cost\ \ after\ \ decontamination\} = \ \ 20unit \times$$
$$\frac{66{,}304kg}{unit} \div \frac{7{,}680kg}{m^3} \div \frac{0.2m^3}{drum} \div 0.8 \times \frac{273.5\ \ million}{drum} - \{20unit \times \frac{66{,}304kg}{unit} \times$$
$$0.15 \div \frac{2{,}230kg}{m^3} \div \frac{0.2m^3}{drum} \div 0.8 \times \frac{273.5\ \ million}{drum} + 20unit \times \frac{66{,}304kg}{unit} \times$$
$$0.85 \div \frac{7{,}680kg}{m^3} \div \frac{0.2m^3}{drum} \times \frac{13.73\ \ million}{drum}\} = 132.6\ \ billion\ \ won \qquad (6.1)$$

Chapter 7. Conclusions and Future Work

7.1 Conclusions

Main goal of this dissertation is to develop a volumetric decontamination process for the volume reduction of intermediate level wastes from PWR decommissioning. Irradiated reactor vessel internals during reactor operation contain about 15 % of long-living activated products by weight. But these long half-life exhibits high specific radioactivity exceeds the limits of LLW. This nature makes them classified into ILW waste and not to be disposed into Gyeongju LILW repository due to its total activity limit.

Nb, Co and Ni are recognized as the target of electrorefining processby ORIGEN-2 code. After that, the reduction and oxidation reaction of elements including Fe in given condition were investigated by the cyclic voltammetry experiments. Basic electrochemical parameters (apparent reduction potential, diffusion coefficient, exchange current density and charge transfer coefficient) are also determined by Cyclic Voltammetry and linear polarization method. Electrorefining, by the pyroprocessing technologies shows decontamination ability of the elements using the redox potential differences among them even if two step processes are required to meet required DF. To scale-up the design decontamination process, overall decontamination process flowsheet was suggested and

some issues with electrorefiner cell design were identified. Issues were solved by new revised cell design and was simulated by CFX computer modeling for verification. A design of electrorefiner was developed and additional cost benefit analysis was performed. This dissertationshows that the developed pyrochemical decontamination process can achieve the reduction effect of the disposal cost by 1/20 and mass of the stored ILW wastes in interim storage by 1/7. Quantitatively, economical effect will be about 132.6 billion won.

Electrochemical decontamination method using molten salt is not yet commercialized, however, it is promising option for decontamination of activated metal wastes. If Fe and Cr are recovered and recycled after decay of Fe^{55}, economical effect will be greater that estimated in this dissertation. Moreover, if separated ILW undergo isotope separation and transmutation as suggested potential roadmap in Chapter 1, dilemma from management of intermediate level decommissioning waste will be solved.

7.2 Future Work

This dissertation suggests introduction of pyrochemical decontamination process for ILW wastes from PWR decommissioning. But, additional electrorefining study for scaling up should be conducted with experimental validation, as follows.

1) Electrorefining study at various applied potential and with suggested new cell design.
2) Optimization of overall decontamination process and design of additional process on flowsheet.
3) Pilot-scale cell design analysis by CFX.

If additional experiments are studied as above, it is expected to help pyrochemical decontamination process commercialized.

Appendix A. ORIGEN-2 INPUT

```
-1
   -1
   -1
   RDA *    Baffle-HJH
   RDA **    CROSS SECTION LIBRARY = PWR.LIB
   CUT         5 1.0E-10 7 1.0E-10 9 1.0E-10 -1
   LIP         0 0 0
   RDA                              DECAY    LIB                XSECT    LIB
VAR. XSECT
   LIB          0        1  2  3          219  220  221        9      50      0      1
9
   RDA           PHOTON LIB
   PHO          101 102 103    10
   TIT       INITIAL  COMP.  OF  UNIT  AMOUNTS  OF  FUEL  AND
STRUCTURAL MAT'LS
   RDA           READ  KHNP  INTERMEDIATE  ALL  INVENTORY
CALCULATION
   INP          -1    1    -1    -1    1    1
   TIT          IRRADIATION OF RVI INTERMEDIATE ALL(BAFFLE
FLUX based)
   MOV          -1 1 0 1.0
```

PCH 1 1 1

HED 1 CHARGE

BUP

IRF 11680 1.59E14 1 2 4 2

BUP

OPTL 8 8 8 8 7 8 7 8 8 8 8 8 8 8 8 8 8 8 8 8 8

OPTA 8 8 8 8 8 8 8 8 8 8 8 8 8 8 8 8 8 8 8 8 8

OPTF 8 8 8 8 8 8 8 8 8 8 8 8 8 8 8 8 8 8 8 8 8

OUT 2 1 -1 0

MOV 2 1 0 1.0

DEC 1.0 1 2 5 2

DEC 3.0 2 3 5 0

DEC 5.0 3 4 5 0

DEC 10.0 4 5 5 0

DEC 15.0 5 6 5 0

DEC 30.0 6 7 5 0

DEC 50.0 7 8 5 0

DEC 70.0 8 9 5 0

DEC 100.0 9 10 5 0

OPTL 8 8 8 8 7 8 7 8 7 8 8 8 8 8 8 8 8 8 8 8 8

OPTA 8 8 8 8 7 8 7 8 7 8 8 8 8 8 8 8 8 8 8 8 8

```
   OPTF          8 8 8 8 7 8 7 8 7 8 8 8 8 8 8 8 8 8 8 8 8
   OUT           10      1       -1      0
   END
4  060000  5.30E+04  250000  1.33E+06  140000  6.63E+05  150000
2.98E+04
4  160000  1.99E+04  280000  6.96E+06  240000  1.33E+07  260000
4.33E+07
4  070000  3.00E+04  030000  8.62E+00  210000  1.99E+00  220000
3.98E+04
4  270000  1.53E+05  290000  2.04E+05  300000  3.03E+04  410000
5.90E+03
4  420000  1.72E+05  470000  1.33E+02  510000  8.16E+02  550000
1.99E+01
4  580000  2.46E+04  620000  6.63E+00  630000  1.33E+00  710000
5.30E+01
4 720000 1.33E+02 900000 6.63E+01    0 0
0
```

Appendix B. REFIN INPUT

Radioactive SS304 PWR internals after 15 years cooling

```
&input1 nelemt=8, a_type=0, temp=773.d0,
   ename = 'Nb', 'fe', 'Cr', 'Co', 'Ni',
'Li', 'Ka' 'Cl',
   stde = 1.4175d0, 1.473d0, 1.751d0, 1.279d0,
1.288d0, 3.900d0, 4.200d0, 0.000d0,
   diffu1= 1.00d-6, 1.00d-6, 1.00d-6, 1.00d-6, 1.000d-6,
1.00d-6, 1.00d-6, 1.0d-6,
   diffu2= 2.6d-6, 1.38d-5, 1.63d-5, 3.74d-5, 1.500d-5,
2.5d-5, 2.5d-5, 2.5d-5,
   curr0 = 1.d-02, 1.d-02, 1.d-02, 1.d-02, 1.d-02,
1.d-06, 1.d-06, 0.D-10,
   zi = 3.0d0, 2.0d0, 2.0d0, 2.0d0, 2.0d0,
1.0d0, 1.0d0, -1.d0,
   tca = 0.5d0, 0.5d0, 0.5d0, 0.5d0, 0.5d0,
0.5d0, 0.5d0, 0.5d0,
   tcc = 0.5d0, 0.5d0, 0.5d0, 0.5d0, 0.5d0,
0.5d0, 0.5d0, 0.5d0,
   catp=-1.5d0,
   anop=-1.5d0,
   ipset= 1,
```

```
   tset=    1000.0d0
   cmaxt= 0.10d0
   aberr=1.d-40,
   rlerr=1.d-15,
&
&input2
   del1=1.0d-3,
   del2=5.0d-3,
   del3=5.0d-3,
   del4=1.0d-3,
      dy=1.0d-3,
   area=4.5d0, 0.95d0,
   vol =0.625d0, 24.69d0, 1.0d0,
&
&INPUT3
   ISTATE=1,
   ITASK=5,
   epslon=5.d-1,
   iopt=1,
   mxstep=1000,
   h0=1.d-5,
   jt=5,
   ml=26,
   mu=26,
```

```
   hmax=600.0d0,
   itol=1,
   rtoli=1.0d-5,
   atoli=1.0d-14,
   iprint=2,
&
&input4
 Can=    8.9501d-05, 6.8187d-01, 2.0703d-01, 1.2602d-03, 1.0975d-01,
3.55d-13, 3.67d-14, 1.65d-15,
 Cms=    4.6624d-13, 1.3218d-02, 4.2305d-13, 4.5389d-15, 4.5288d-15,
7.1466d-02, 2.7979d-01, 6.3552d-01,
 Cca=      0.000d-20,   0.000d-20,   0.000d-20,   0.000d-20,   0.000d-20,
0.000d-20, 0.000d-20, 0.000d-20,
&
&input5
 mass=5.0d0, 40.014d0, 1.0d0,
 gatom=92.906d0, 55.847d0, 51.996d0, 58.933d0, 58.693d0, 6.941d0,
39.098d0, 35.453d0,
&
```

Bibliography

[1]IAEA Power Reactor Information System (2019, Jan, 1th), Operational Reactors by Age, World Statistics. Available: https://www.iaea.org/PRIS/WorldStatistics/OperationalByAge.aspx

[2]Preparation program at the pre-decommissioning phase for the D&D of the Kori-1 Nuclear Power Plant from KHNP presentation material at IAEA conference(2016.08.31).

[3] OECD/NEA, Decontamination Techniques Used in Decommissioning Activities.

[4] Byeong-Yeon Min, Ki-Won Lee, Gyoung-Su Yun and Jei-Kwon Moon, 2012, Current Status and Futrure Issues for Melt Decontamination of Decommissioning Metal Wastes Generated from Nuclear Facilities, Proceedings of the Korean Radioactive Waste Society SPRING 2013, Vol. 29, No. 7, pages 603~615.

[5] WIKIPEDIA, Cyclic Voltammetry, Available : https://en.wikipedia.org/wiki/Cyclic_voltammetry

[6]https://sop4cv.com/chapters/EvaluatingElectrochemicalReversibility.html

[7] Byung Gi Park and Il Soon Hwang,1999, Simulation of electrorefining process using time-dependent multi-component electrochemical model: REFIN, Proceedings of the Korean Nuclear Society autumn meeting.

[8] EPRI, 2012, Trace Impurities and Activation Products in Base Metal, 2012 Technical Report 1025313, North Oaks, U.S.

[9] J. Park, S. Choi, S. Sohn, and I. S. Hwang, Cyclic Voltammetry on Zr, Sn, Fe, Cr and Co in LiCl-KCl Salts at500℃ for Electrorefining of Irradiated Zircaloy-4 Cladding, Journal of The Electrochemical Society, Vol. 164, No. 12,pp.744-751, 2017.

[10] Pyeong-Hwa Kim, A Study on ElectrochemicalDecontamination of Irradiated Zr-Nb Alloys in LiCl-KClEutectic Molten Salts, Master dissertation, 2016.

[11] M. Iizuka, T. Inoue, O. Shirai, T. Iwai, and Y. Arai,Application of normal pulse voltammetry to on-linemonitoring of actinide concentrations in molten saltelectrolyte, Journal of nuclear materials, Vol. 297, pp.43-51,2001.

[12] 국회예산정책처, 해외 원자력 발전 및 방사성 폐기물 처리 관련 규제의 사례연구, 2013

초 록

현재, 454기의 원자력 발전소가 전세계적으로 운영 중에 있으며 전체 발전량의 약 11%를 차지하고 있다. 이 중 약 66%의 원자력 발전소는 30년 이상 가동되었으며, 이와 같은 노후원전의 비율이 앞으로 지속적으로 증가할 것으로 예상된다. 국내의 경우, 이미 고리 1호기의 영구정지가 시행되었으며 2030년 전에 7기의 가압경수로형 원자로의 설계수명이 만료가 될 예정이다. 이에 따라 원자력 발전소 해체 준비 필요성이 증가하고 있으며 해체에 따라 발생할 중저준위 방사성 폐기물 관리도 중요해지고 있다. 이 중, 중준위 금속 폐기물이 발생하는 양은 약 66톤으로 주로 방사화 노내 구조물로 이루어져 있다. 노내 구조물은 스테인리스강으로 이루어져 있으며 노심 주변부로써 높은 중성자속에 장기간 노출되어 있다. 스테인리스강이 방사화됨으로써 C^{14}, Nb^{94}, Ni^{59}, Ni^{63}과 같은 장수명 방사성 핵종 및 Co^{60}과 같은 단수명 방사성 핵종이 발생하게 된다. 하지만 현행 규정 상 방사화 노내 구조물과 같이 장수명 방사성 핵종이 다량 포함된 중준위 방사성 폐기물은 경주 중저준위 방사성 폐기물 처분장의 방사능 총량 규제 기준 한계에 의해 처분될 수 없다. 따라서, 우리나라뿐만 아니라 대다수의 국가들이 관련시설의 임시저장소에 보관 중이며 고준위 방사성 폐기물 혹은 사용후핵연료 처분장의 건설을 기다리고 있는 상황이다. 이를 해결하기 위한 장수명 방사성 핵종을 포함한 중준위 금속 폐기물들의 제염기술 개발이 필요하다.

ORIGEN-2를 활용하여 가압경수로 노내 구조물이 32년 유효전출력기간을 가정하여 모델링한 결과, 냉각기간이 15년 지난 뒤 위 핵종들의 방사능 농도는 C^{14}(1.83E+06Bq/g), Nb^{94}(2.88E+04Bq/g), Ni^{59}(5.40E+06), Ni^{63}(1.05E+07Bq/g), Co^{60}(1.35E+09Bq/g)으로 중준위 방사성 폐기물로 평가된다. 국내 가압경수로형 원자로 해체 후 나올 중준위 노내 구조물들이 모두 경주 중저준위 방사성 폐기물 처분장에 처분되기 위해 요구되는 제염계수는 각각 8.2, 259.1, 73.0, 94.7, 36.6이다.

본 논문에서 제시하는 제염공정은 방사화 핵종을 체적제염시킬 수 있으며, 이론적으로 2차폐기물 발생량이 0인 용융염 기반 전해정련이다. 용융염은 불화물(LiF-KF)보다 운전온도가 낮고 부식문제가 적은 염화물(LiCl-KCl)을 선택하였고 핵종들 사이 환원전위차를 이용하여 장수명 핵종들을 남기고 산화경향성이 큰 Fe과 Cr을 회수하는 실험을 수행하였다.

전해정련 실험 전 주요 원소들(Fe, Co, Ni, Cr)의 LiCl-KCl 용융염 내 산화환원 거동을 알아보기 위해 각 원소들의 염화물을 녹인 후 500℃에서 순환전압전류법을 수행하였다. Cr을 제외한 모든 핵종들은 한 개씩의 산환환원피크 쌍을 보였으며, 단순한 거동을 보였다. Cr은 두 쌍의 산화환원피크를 보였으나, Fe의 산화피크가 -0.2~-0.1V[vs. 1 wt. % Ag/AgCl] 에서 발생하는 것으로 보았을 때, Cr^{2+}와 Cr^{3+} 사이의 산화거동은 무시할 수 있을 것으로 판단했다.

순환전압전류법을 통해 나온 결과를 토대로 각 원소별 Apparent reduction potential과 용융염 내 확산 계수를 획득하였다. 또한, Linear

Polarization Method를 통해 각 핵종들의 교환 전류 밀도 및 전하전달계수를 획득함으로써 관련 연구를 위한 데이터베이스를 구축하였다. 구축된 데이터베이스와 1-D 시간 종속 전기화학 모델링코드 REFIN을 활용하여 전해정련 모델링을 수행함으로써 전해정련을 통한 제염계수 확보가능성을 평가하였다. 전해정련을 통해 Nb, Co에 대한 제염계수는 확보가능하다는 것을 보였으며, Ni의 경우 2번의 반복과정을 거치면 제염계수를 달성할 수 있다.

모델링 결과의 검증을 위해 전해정련 실험을 수행하였다. 실험 조건은 LiCl-KCl-3 wt. % $FeCl_2$ 용융염을 사용하였고, 양극엔 스테인리스강 막대를 사용하였다. 실험 중 양극, 음극에서 떨어져 나올 수 있는 금속들을 회수 혹은 금속 물질에 의한 오염 방지를 위해 양 극 주변에 용기를 설치하였다. 양극에 걸리는 전위가 -0.2V[vs. 1 wt. % Ag/AgCl], -0.2V[vs. 1 wt. % Ag/AgCl], -0.1V[vs. 1 wt. % Ag/AgCl], 0V[vs. 1 wt. % Ag/AgCl]로 다르게 주어 3번 수행하였다. 전해 정련 셀 내 음극표면, 음극 용기 내부, 양극 용기 내부, 용융염들의 ICP-MS 분석을 수행하였으며, 음극표면의 전착물을 확인하기 위해 XRD 분석을 수행하였다. 분석 결과 음극표면에 Fe가 금속상태로 전착되는 것이 확인되었으며, 양극 인가 전위가 증가하면서 Co, Ni의 제염계수가 감소하는 것을 확인되었다. 이는 양극 인가 전위의 증가로 Fe뿐만이 아닌 Co, Ni의 산화 피크가 일정 부분 포함되면서 양극에서 녹아나와 전착이 된 것으로 예상된다. 하지만 3가지 실험 모두 전해정련 공정이 2번 반복 수행되었을 때, 요구되는 제염계수를 만족시킬 수 있는 것으로 확인되었다.

실제 공정 내에서 한계전류와 확산층 제어를 위해 회전전극을

사용한다는 점을 고려하여 셀 내 용기를 설치한 것이었다. 하지만 전해정련 실험 중 한계전류의 형성이라는 문제점을 확인할 수 있었고 이를 보안하기 위해 CFX코드를 활용하여 새로운 셀 디자인을 설계하였다. 셀 내 추가적인 용기의 디자인을 미세 다공성 구조로 모델링하여 유체 내 입자 거동 해석과 전압 강하에 대한 시뮬레이션을 수행하였다. 미세 다공성 용기를 통해 전압 강하는 2배 이상의 효율을 보였으며, 회전 전극에 의한 유체 거동에 따른 입자의 음극 용기 내 이탈이 효율적으로 제어될 수 있음을 확인하였다.

본 논문의 연구결과를 통해 파일럿 규모의 전해정련로를 제작한다면 경제적으로 1320 억원 이상의 효과를 나타낼 것으로 예상된다.

주요어: 노내 구조물, 해체 폐기물, 스테인리스강 재활용, 용융염, 전해정련

학 번: 2017-24704